

Interactive comment on “Continental pollution in the Western Mediterranean Basin: vertical profiles of aerosol and trace gases measured over the sea during TRAQA 2012 and SAFMED 2013” by C. Di Biagio et al.

At first, we would like to thank the reviewer for having carefully read the revised paper and provided valuable comments which helped to improve the quality of the manuscript. We have taken into consideration all the questions raised by the reviewer, and changed the paper accordingly. The details of our changes are highlighted in the text. The point by point answers to Reviewer #1 are provided in the following.

Anonymous Referee #1

Review of the manuscript “Continental pollution in the Western Mediterranean Basin: ... by Di Biagio et al. Revised version

The manuscript improved compared to the previous version and several errors were removed. However the current version still has a few deficiencies that should be corrected prior to publication. My comments refer to the version of the manuscript with ‘track changes’ option.

Specific comments:

Page15, line 83/84. Introduction. The statement that a large set of observations in the last decades permits to characterize a detailed view of pollution aerosols in the surroundings of the Western basin is in contradiction to the answer to my question of ‘typical’ for pollution aerosols section 5.3. These numbers are obviously not as well-known as stated in the Introduction. However, a few recent measurement campaigns could shed some more light on this issue.

As stated in lines 59-62 of the Introduction “A number of studies have investigated the dynamics of pollution export over the Western basin with the aim of characterizing the impact of anthropogenic emissions over this region. Most of these studies have been conducted in continental coastal areas and provide information on the vertical distribution of aerosols and their properties mainly close to local pollution sources.”. So, mostly, the characterization available in the literature focusses on dynamical and seasonal processes controlling the export of pollution in the Western basin. Even if some information are available on the particle size distribution and optical properties of these aerosols (e.g., Mallet et al., 2003 and 2005; Perez et al., 2004), a lack of knowledge exists. With the aim of putting this more in evidence in the paper, the Introduction has been modified as:

“The large set of observations conducted in the last decades in the Western Mediterranean has permitted mostly to characterise the dynamics and processes of pollution export in the surroundings of the basin. However, at the present time we miss an extensive representation of the mean load, distribution, and physico-chemical and optical properties of the atmospheric aerosols, as well as trace gases distribution, in the whole region, in particular over the remote sea. In addition, there is a significant lack of observations over some key areas, as for example the Gulf of Genoa, directly under the influence of the outflow from the highly polluted Po Valley (Velchev et al., 2011).”

Section 3. Measurements and methods, page 18, lines 152 to 158. Both instruments, the GRIMM and the PCASP are optical particle spectrometers OPS's, to OPC's.

The terminology has been corrected as suggested by the reviewer.

Section aerosol scattering coefficient, line 173. Instrument was calibrated prior to each campaign.

The correction has been made.

Section 3.2 Aerosol number concentration. The PCASP seems to have a problem either with calibration or inlet losses. Even when the authors have the impression that the subsequent analysis is not affected, they should have an idea what could be the reason. The different options have consequences for the size distribution measurements with this instrument.

It is not clear based on the data and the information that we have if the PCASP problem between 0.4 and 1.0 μm comes from a calibration issue or others, like for example a reduced sensitivity of this instrument in this size range. An inlet losses problem has to be excluded since the PCASP is installed outdoor, on the left side of the aircraft fuselage.

What we observe from the data is a very good agreement with the GRIMM below 0.4 and above 1.0 μm , which indicates that in these ranges the PCASP data are accurate. So, excluded the problem between 0.4 and 1.0 μm , which is discussed in the text, as well as taken into account for the possible uncertainty on the calculated dN_{Acc} , the measurements of the PCASP can be assumed to be correct.

Section 4. Meteorological conditions, aerosol load, and pollution export regimes, page 24, line 297: The authors mention a profile V18, which is included in Table 1, but neither in Figure 1 nor in any of the other figures.

V18 was a high-altitude flight used to perform exclusively lidar measurements over the region; no profiles are available during this flight. We have eliminated V18 from line 292. For the reader's sake we have also specified in Table 1 the flights for which vertical profiles were not performed.

Line 305, Flights V24-V25-V26 were flown within two days of a certain meteorological situation, profile V31 one week later, still in the same meteorological situation?

This part has been rewritten as "Additionally, flight V31 sounded the atmospheric structure close to the Spanish coasts reaching the southern urban area of Valencia. The flight was performed one week later (10 July) under a similar meteorological condition characterized by south-westerly winds favouring the export from the Iberian Peninsula towards the basin"

Section 5.1, Vertical profiles of aerosol concentration, page 26, line 354 and also in the Abstract. The numbers given for the coarse aerosol mode are way too high. 4000 scm^{-3} would be probably possible directly in a heavy pollution plume, but even Saharan Dust layers are about one order of magnitude lower in concentration.

The reviewer is correct and by looking at Figure 6 the $\text{dN}_{\text{Coarse}}$ is multiplied by 100 to let the plot more easily readable. So, the concentrations are a factor 2 lower than shown in the plot and stated in the text. I have corrected the numbers in the text.

Also, in the caption of Figure 6 I have added a note on this.

Page 28, line 393. ‘This suggests that the export towards the basin favours the redistribution of the pollution plumes along the vertical.’ This statement needs a further description of a possible process.

The description of all the possible processes, as observed in the Western basin, is already reported in the lines 393-419:

“Because of mixing in the BL, measured concentrations within the BL can be as high as those observed close to the surface over the continents. Values of dN as high as in the BL are observed in the FT because of transport in specific conditions, as discussed below.

The observations of aerosol profiles obtained during TRAQA and SAFMED are representative of the complex transport regimes which characterizes the export towards the Western basin and that is mostly determined by the interaction between regional meteorology and local dynamics (e.g., Gangoiti et al., 2001). A first example is associated to the measurements in the area of Barcelona. As discussed in Pérez et al. (2004) the presence of mountains up to ~500-3000 m altitude a few kilometres inland favours, during summertime, the recirculation of pollutants along the coasts of Spain. In these cases, the aerosols emitted at the surface in coastal areas are transported inland and uplifted by sea breezes and mountain winds then the plumes are re-injected at different altitudes and distances from the coast. During the TRAQA flights V24, V25, and V26, under the influence of pollution outflow from the Barcelona area, we detected the presence of aerosol layers with elevated concentrations ($dN_{Acc} \sim 2000-3000 \text{ scm}^{-3}$) up to 3500 m altitude at a distance of ~30 to 250 km from the coast of Spain. Another example of complex dynamics linked to coastal orography is that associated to the export from northern Italy and the Po Valley towards the Gulf of Genoa. The presence of the Apennine Mountains close to the Ligurian coasts (max elevation ~1500-2000 m) causes the uplift of continental air masses so determining the injection of aerosol plumes at different altitudes both inside and outside the BL. Examples are given by flights V19, V21 and V52 for which pollution aerosols from northern Italy are measured up to ~2000-3000 m altitude throughout the Gulf of Genoa. Finally, another meteorological condition which largely influences the aerosol export and distribution over the Western Mediterranean is the Mistral/Tramontane wind regime. Under the influence of the Mistral flow, atmospheric aerosols can be dispersed as far as hundreds of kilometres over the open sea, as discussed by Salameh et al. (2007). Examples are given in profiles V20 and V28, performed at more than 100 km from the French coasts, for which pollution layers associated to a Mistral flow are measured up to 2000-3000 m altitude.”

Section 5.3, O₃/CO ratios and variability: In my first review I asked for a more details on the time resolution of the instruments and a possible mismatch within the data. This is especially important in vertical profile measurements when concentrations change more rapidly than in horizontal flights. In fact the Nedelec et al paper gives a 30 second time delay for the measurements of CO, the ozone instrument is not described, but a 4 second time resolution is given. In the profile this faster response can be seen in an earlier change of the ozone compared to the CO and especially the ratio of ozone to CO could be less noisy after correction.

As discussed in the first round of the revisions, we have checked and there is not a mismatch between the CO and the O₃ data. Concerning instead the reviewer comment on the different time resolution of CO and O₃ measurements, unfortunately we do not have enough information on the

instrument to correct the noise possibly arising from this effect. However, to evidence this possible factor of uncertainty, we have added a comment on this in the text (lines 456-458):

“The $\Delta O_3/\Delta CO$ ratio is highly noisy and this is due in part to the noise in the CO data, and in part also possibly associated to the slight mismatch between CO and O₃ caused by their different time resolution (30 s for CO and 4 s for O₃).”

Section 5.4, Layers with enhanced Aitken mode particle numbers, page 35, line 565 to 575

Investigations of new particle formation require a details size distribution measurement in the size range below 30 nm. An SMPS system would be necessary. As the authors do not have this instrument on board this section is highly speculative and should be omitted.

The whole text in lines 565-575 is not intended to be speculative. We observe the presence of enriched dN_{Aitken} layers in some cases and we propose some explanations based on the information we have available during the flights. We explicitly state in the text that we do not have the adapted resolution in size measurements to clearly discriminate NPF events. Moreover, we claim that the discussion is only intended to provide a qualitative indication of the possible occurrence of NPF.

Given the importance of NPF and ultrafine particles in several processes, as well as the lack of aerosol characterization in the Western Mediterranean basin, we consider very useful to maintain this part of the discussion in the text. Then, at the same time, we also assume that all the necessary information to completely evaluate our discussion/conclusions have been given to the reader.

New table 2, Page 47, line 917 to 927. In the citation Junkermann et al, line 925 correct the word September.

The correction has been made.

Editor comments

Following review of your revised manuscript, I would like to invite you to submit a further revised manuscript, taking onto account the reviewer's comments (attached in the pdf). The revisions requested are now minor, so thank you for the changes you have made so far.

By way of further clarification to the changes requested I have a few comments:

1. Please adjust the Introduction to better reflect the lack of detailed information on the character of aerosols in the Western Basin.

This part of the Introduction has been modified as suggested by the Reviewer.

2. I think the reviewer's second comment is meant to say that you should use the terms optical particle spectrometer for the GRIMM and PCASP instruments rather than optical particle counters.

The terminology has been corrected as suggested by the reviewer.

3. Whilst the possible mismatch between CO and Ozone instrument time resolution may lead to a large uncertainty and probably high noise in the O₃/CO ratios, it is recognised that this is not really

important for the general results of the manuscript. However, please at least comment on this source of error in these ratios.

A comment on this has been added in lines 456-458.

Please also correct the caption to Figure 7 “Carbone” should be “Carbon”.

The correction has been made.

1 **Continental pollution in the Western Mediterranean basin: vertical profiles of**
2 **aerosol and trace gases measured over the sea during TRAQA 2012 and**
3 **SAFMED 2013**

4 C. Di Biagio¹, L. Doppler^{2,3,4}, C. Gaimoz¹, N. Grand¹, G. Ancellet², J.-C. Raut², M. Beekmann¹, A.
5 Borbon¹, K. Sartelet⁵, J.-L. Attié^{6,7}, F. Ravetta², and P. Formenti¹

6 (*corresponding author: claudia.dibiagio@lisa.u-pec.fr)

7
8 ¹ *LISA, UMR CNRS 7583, Université Paris Est Créteil et Université Paris Diderot, Institut Pierre*
9 *Simon Laplace, Créteil, France*

10 ² *Sorbonne Universités, UPMC Univ. Paris 06; Université Versailles St-Quentin; CNRS/INSU,*
11 *LATMOS-IPSL, Paris, France*

12 ³ *Freie Universität Berlin, Berlin, Germany*

13 ⁴ *Deutscher Wetterdienst, Meteorological Observatory Lindenberg, Germany*

14 ⁵ *CEREA, Joint Laboratory École des Ponts ParisTech – EDF R & D, Université Paris-Est, 77455*
15 *Marne la Vallée, France*

16 ⁶ *Laboratoire d'Aérodologie, University of Toulouse, UMR 5560 CNRS, France*

17 ⁷ *CNRM GAME UMR 3589 CNRS, METEO-FRANCE*

18
19 **Abstract**

20 In this study we present airborne observations of aerosol and trace gases obtained over the sea in the
21 Western Mediterranean basin during the TRAQA (TRansport and Air QuAlity) and SAFMED
22 (Secondary Aerosol Formation in the MEDiterranean) campaigns in summers 2012 and 2013. A
23 total of 23 vertical profiles were measured up to 5000 m above sea level over an extended area

24 (40°-45°N latitude and 2°W-12°E longitude) including the Gulf of Genoa, Southern France, the
25 Gulf of Lion, and the Spanish coast. During TRAQA and SAFMED the study area experienced a
26 wide range of meteorological conditions which favoured the pollution export from different sources
27 located around the basin. Also, several events of dust outflows were measured during the
28 campaigns. Observations from the present study show that continental pollution largely affects the
29 Western Mediterranean both close to coastal regions and in the open sea as far as ~250 km from the
30 coastline. The measured aerosol scattering coefficient varies between ~20 and 120 Mm⁻¹, while
31 carbon monoxide (CO) and ozone (O₃) mixing ratios are in the range of 60-165 ppbv and 30-85
32 ppbv, respectively. Pollution reaches 3000-4000 m in altitude and presents a very complex and
33 highly stratified structure characterized by fresh and aged layers both in the boundary layer and in
34 the free troposphere. Within pollution plumes the measured particle concentration in the Aitken
35 (0.004-0.1 μm) and accumulation (0.1-1.0 μm) modes is between ~~~3400~~ and 5000-6000 scm⁻³
36 (standard cm⁻³), which is comparable to the aerosol concentration measured in continental areas
37 under pollution conditions. Additionally, our measurements indicate the presence of highly
38 concentrated Aitken layers (10000-15000 scm⁻³) observed both close to the surface and in the free
39 troposphere, possibly linked to the influence of new particle formation (NPF) episodes over the
40 basin.

41

42 **1. Introduction**

43 Atmospheric aerosols play an important role on climate through their participation to several
44 chemical, dynamical, and radiative processes. At present, still large uncertainties persist in the
45 estimation of the aerosol direct and indirect effects mainly due to the difficulty of fully
46 characterizing their spatial and vertical distribution and properties (Boucher et al., 2013).

47 The Mediterranean region is a complex area where atmospheric aerosols of different origins and
48 types may be found (Pace et al., 2006; Kallos et al., 2007; Gkikas et al., 2012). High levels of

49 anthropogenic aerosol particles and pollutants are measured in the Mediterranean (Lelieveld et al.,
50 2002), which is also indicated as one of the main hot spots for air quality issues (Monks et al.,
51 2009).

52 The North-Western part of the Mediterranean basin, due to its proximity to highly polluted
53 industrialized areas (such as the Po Valley in northern Italy and the Fos/Berre in southern France)
54 and large coastal cities (Barcelona, Genoa, Marseilles, Nice, or Valencia), is frequently affected by
55 continental outflows and severe pollution episodes (Mallet et al., 2005; Pérez et al., 2008; Pey et al.,
56 2010). The strength of these episodes is particularly intense during summer when stable
57 meteorological conditions and the high level of insolation promote photochemical reactions and the
58 build-up of ozone and other pollutants (e.g. Millán et al., 2000).

59 A number of studies have investigated the dynamics of pollution export over the Western basin with
60 the aim of characterizing the impact of anthropogenic emissions over this region. Most of these
61 studies have been conducted in continental coastal areas and provide information on the vertical
62 distribution of aerosols and their properties mainly close to local pollution sources. They include
63 ground-based observations with lidars (Soriano et al., 2001; Pérez et al., 2004; Ancellet and
64 Ravetta, 2005), and airborne campaigns, such as MECAPIP (MEso-meteorological Cycles of Air
65 Pollution in the Iberian Peninsula) and RACAPMA (RegionAl Cycles of Air Pollution in the west
66 central Mediterranean Area) in coastal Spain (Millán et al., 1996 and 1997), and ESCOMPTE
67 (Experience sur Site pour Contraindre les Modeles de Pollution atmospherique et de Transport
68 d'Emissions) in Southern France (Drobiniski et al., 2007). The results of these studies have
69 highlighted the important role of pollution in modulating the atmospheric composition in this part
70 of the basin, as well as the high variability of the aerosol distribution and properties in link to
71 different export conditions (Flamant and Pelon, 1996; Soriano et al., 2001; Mallet et al., 2005). In
72 particular, the interaction between synoptic circulation and local dynamics, such as orography and
73 sea breezes, has been shown to strongly impact the vertical distribution, layering, and aging of

74 particles along coastal regions (e.g. Millan et al., 1997; Gangoiti et al., 2001; Pérez et al., 2004;
75 Velchev et al., 2011).

76 The capability of reproducing this complexity by air quality models represents a real challenge
77 (Jimenez et al., 2006; Jiménez-Guerrero et al., 2008), and experimental observations gives a
78 fundamental support to test the performances of the model outputs over the Western Mediterranean
79 environment.

80 The large set of observations conducted in the last decades in the Western Mediterranean has
81 permitted mostly to ~~acquire a detailed characterisation~~ characterise the dynamics and processes of
82 pollution export aerosols in the surroundings of the ~~Western~~-basin. However, at the present time we
83 miss an extensive -representation of the mean aerosol-load, distribution, and physico-chemical and
84 optical properties of the atmospheric aerosols, as well as trace gases distribution, in the whole
85 region, in particular over the remote sea. In addition, there is a significant lack of observations over
86 some key areas, as for example the Gulf of Genoa, directly under the influence of the outflow from
87 the highly polluted Po Valley (Velchev et al., 2011).

88 In this study we present -measurements of aerosols and trace gas vertical profiles acquired during 24
89 scientific flights performed with the ATR-42 French research aircraft during the TRAQA
90 (TRansport and Air QuAlity) and SAFMED (Secondary Aerosol Formation in the MEDiterranean)
91 campaigns in summers 2012 and 2013 in the framework of the Chemistry-Aerosol Mediterranean
92 Experiment (CHARMEX, <https://charmex.lsce.ipsl.fr/>). The TRAQA and SAFMED flights
93 explored an extended region of the Western Mediterranean basin between 40°-45°N latitude and
94 2°W-12°E longitude including the Gulf of Genoa, Southern France, the Gulf of Lion, and the
95 Spanish coasts. Measurements were performed over the sea at various distances from the coastline
96 with lidar and in situ instruments. During TRAQA and SAFMED the Western basin was under
97 diverse synoptic conditions which led to the occurrence of different pollution export regimes

98 (Mistral/Tramontane events, outflow from the Po Valley and the Iberian Peninsula) and allowed
99 sampling atmospheric aerosols of different origin and types.

100 The main objective of the present work is to provide observations of the vertical distribution of
101 aerosols and trace gases related to the export of anthropogenic pollution at the regional scale of the
102 Western Mediterranean basin. The detailed knowledge of the vertical structure of the atmosphere is
103 very important to understand the impact of continental pollution over the basin.

104 The paper is organized as follows: in Sections 2, 3, and 4 we describe the flight trajectories and
105 strategy during TRAQA and SAFMED, the in situ measurements carried out on board the ATR-42
106 aircraft, and the meteorological conditions observed during the campaigns. In Sect. 5 we present the
107 results. The aerosols and trace gases vertical profiles are shown in Sections 5.1 and 5.2. Section 5.3
108 is dedicated to analyse the variability of the pollution plume composition and atmospheric structure
109 also in link with the different outflow conditions. Airborne measurements in presence of layers with
110 high concentrations of fine particles are discussed in Section 5.4. The main conclusions are reported
111 in Section 6.

112

113 **2. Overview over flights**

114 Figure 1 shows the trajectories of the flights performed during the TRAQA (20 June-13 July 2012)
115 and the SAFMED (24 July-1 August 2013) campaigns. Research flights were performed with the
116 SAFIRE (Service des Avions Français Instruments pour la Recherche en Environnement,
117 <http://www.safire.fr/>) tropospheric aircraft ATR-42. The aircraft has a maximum endurance of 4 h.
118 The flight altitude ranges between a minimum of ~60 m over the sea, to a maximum of ~5000 m
119 above sea level (a.s.l.). The aircraft was based in Toulouse (43°36'N, 1°26'E, France) during
120 TRAQA and in Genoa (44°24'N, 8°55'E, Italy) during SAFMED. Twenty-four flights for a total of
121 ~75 hours of data have been collected. Seventeen of the twenty-four flights presented in the paper
122 were performed during TRAQA (flight numbers V16 to V32) and 7 during SAFMED (V46 to

123 V52). All flights were carried out during daytime, when light-induced chemistry favours the
124 pollution levels. Frequently, two flights per day, with intermediate stops in different airports in
125 Southern France, Corsica, and Sardinia, were performed. The majority of flights were over the sea,
126 with some exceptions investigating inland areas in Southern France and central Italy. Main
127 information concerning the TRAQA and SAFMED flights is summarized in Table 1.

128 The general flight strategy consisted in plane flights with lidar observations and vertical
129 ascents/descents to sound the vertical atmospheric column (from ~60-100 m to 3000-5000 m a.s.l.)
130 and identify main meteorological and aerosol features, followed by straight levelled runs (SLRs)
131 within the detected aerosol layers. In this study we focus on vertical profiles data. A total of 23
132 profiles were acquired in 20-30 minutes each by performing a spiral trajectory ~10-20 km wide.
133 Fig. 1 also identifies the geographical position of each sounding. As shown in Fig. 1 the profiles
134 were performed at different distances from the coastline, from a minimum of ~5-10 km for V31 and
135 V32 to more than ~250 km for V20 and V25, and covered almost all the different sectors of the
136 Western basin.

137

138 **3. Measurements and methods**

139 The basic equipment of the ATR-42 aircraft includes sensors for the measurements of
140 meteorological parameters (pressure, temperature, relative humidity, wind components), radiative
141 fluxes (down- and up-welling shortwave and longwave radiation), and carbon monoxide (CO) and
142 ozone (O₃) mixing ratios.

143 Aerosol sampling was performed using the AVIRAD system (Formenti et al., 2011). AVIRAD is an
144 iso-axial and iso-kinetic inlet which, at the normal cruise speed of the ATR-42 (~93 m s⁻¹), samples
145 air at a volumetric flow of ~350 l min⁻¹. The 50% passing efficiency of the inlet was tested to be 12
146 μm diameter. Various sampling lines depart from AVIRAD to connect to different instruments
147 mounted inside the aircraft cabin: (i) a 3-wavelength nephelometer (TSI Inc., model 3563) for the

148 measurement of the dry particle volume total scattering (σ_s) and hemispherical backscattering (σ_{bs})
149 coefficients at 450, 550, and 700 nm; (ii) a 7-wavelengths aethalometer (Magee Sci., model AE31)
150 for the measurement of the particle absorption coefficient (σ_a) at 370, 470, 520, 590, 660, 880, and
151 950 nm; (iii) an optical particle ~~counter~~-spectrometer (GRIMM Inc., model 1.129) for the
152 measurement of the particle number concentration over 32 size classes between 0.3 and 32 μm in
153 diameter; (iv) a Condensation Particle Counter (CPC, TSI Inc., model 3775) for the measurement of
154 the total particle number concentration in the diameter range 0.004-3.0 μm ; and (v) 3 lines for
155 aerosol sampling on filter membranes and a 4-stage cascade impactor (Dekati Inc) to measure the
156 bulk and size-segregated particle composition. In addition, the ATR-42 was equipped with a
157 Passive Cavity Aerosol Spectrometer Probe (PCASP, model 100X) optical particle ~~counter~~
158 spectrometer for the measurement of the aerosol number concentration over 31 size classes between
159 0.1–3.0 μm . The PCASP was installed outside the cabin on the left side of the aircraft fuselage.

160 In this study we consider measurements of the (i) aerosol scattering coefficient from the
161 nephelometer, (ii) particle concentration from the CPC and PCASP instruments (GRIMM data are
162 not considered since they are available only below ~350 m during TRAQA), (iii) CO and O₃ trace
163 gases from the MOZART analyser, and (iv) meteorological parameters from the ATR-42 sensors. A
164 more detailed description of the nephelometer, CPC, PCASP, and MOZART measurements and
165 their data analysis is provided in the following sections.

166 The present analysis is based only on measurements obtained in cloud free conditions.

167

168 **3.1 Aerosol scattering coefficient**

169 A three-wavelength integrating nephelometer has been used to measure the dry particle volume
170 total scattering (σ_s) coefficient at 450, 550, and 700 nm. The sampling flow rate was 30 l min⁻¹.
171 Data were acquired at 6 s resolution during TRAQA and 1 s resolution during SAFMED. The
172 instrument was calibrated prior to each campaign with free-particle air and CO₂ as gases of low and

173 high known scattering coefficient. Nephelometer measurements have been corrected for angular
174 truncation and Lambertian non-idealities by applying the formulae by Anderson and Ogren (1998).
175 The measurement uncertainty on σ_s is calculated taking into account for the photon counting, gas
176 calibration, and angular corrections uncertainties (Anderson et al., 1996; Anderson and Ogren,
177 1998). The total uncertainty on σ_s is estimated to be lower than 10% at the three wavelengths.

178 The nephelometer measured the scattering coefficient in dry air conditions. This is due to the
179 heating of the airflow while entering the aircraft cabin and the temperature in the cavity of the
180 instrument. The relative humidity measured during the flights inside the nephelometer was <25% in
181 more than ninety percent of cases, with values up to ~40% occasionally observed at very low
182 altitudes (<200 m) over the sea surface. A possible underestimation of the scattering coefficient
183 may thus occur in case of hygroscopic aerosols, especially under high relative humidity conditions
184 in the atmosphere.

185 The particle scattering Ångström exponent (α_s) has been calculated from spectral nephelometer
186 measurements with a power-law fit of the measured scattering coefficients versus wavelength.

187

188 **3.2 Aerosol particle number concentration**

189 The vertical profiles of the total particle number concentration in the Aitken (dN_{Aitken} , 0.004-0.1
190 μm), accumulation (dN_{Acc} , 0.1-1.0 μm) and coarse (dN_{Coarse} , >1.0 μm) modes have been obtained
191 by combining CPC and PCASP data. The CPC and the PCASP measured at a sample flow of 1.5
192 and 0.06 l min^{-1} , respectively, and with a time resolution of 1 s for the PCASP and 5 s and 1 s for
193 the CPC during TRAQA and SAFMED, respectively.

194 The PCASP was factory calibrated with monodisperse polystyrene sphere latex (PSL) whose
195 complex refractive index at the instrument operating wavelengths (632.8 nm) is 1.59-0i. The
196 measured sphere-equivalent optical diameter has been converted to a sphere-equivalent geometrical

197 diameter (D_g) by taking into account the complex refractive index of the sampled aerosol (Liu and
198 Daum, 2000). Given that in the very large majority of cases the aerosol sampling during TRAQA
199 and SAFMED was associated to the export of pollution plumes, only pollution aerosols have been
200 considered for PCASP correction. Note that these data are not optimized for dust or marine aerosol
201 observations. A large interval of values ($n \sim 1.50-1.72$, $k \sim 0.001-0.1$ for UV-visible wavelengths) are
202 reported in the literature for the real and the imaginary parts of the refractive index for
203 anthropogenic aerosols over Europe (e.g., Ebert et al., 2002 and 2004; Müller et al., 2002; Mallet et
204 al., 2003 and 2011; Chazette et al., 2005; Raut and Chazette, 2008). For our calculations at 632.8
205 nm we have fixed the imaginary part of the refractive index to 0.01, thus representing a mean
206 absorbing aerosol, and then we have varied the real part between its minimum (1.50) and maximum
207 (1.72) reported value. D_g is then set at the mean \pm one standard deviation of the values obtained for
208 the different values of n . We assume in these calculations that the refractive index does not vary
209 with height. After refractive index correction the D_g range for the PCASP becomes 0.10-4.47 μm ,
210 with an uncertainty between 1 and 25%. The smallest and the largest size bins of the PCASP, for
211 which the minimum and maximum edges respectively are not defined, have been excluded from the
212 datasets, thus reducing the PCASP D_g range to 0.11-4.17 μm .

213 Once corrected for the refractive index, PCASP data have been combined with those from the CPC
214 to calculate dN_{Aitken} , dN_{Acc} , and dN_{Coarse} . Values for dN_{Acc} and dN_{Coarse} are obtained by integrating
215 the PCASP number concentrations in the 0.1-1.0 μm and 1.0-4.17 μm ranges, while dN_{Aitken} is
216 estimated as the difference between CPC concentration and the integral of PCASP data between 0.1
217 and 3.0 μm . The comparison between the PCASP and the GRIMM below 350 m altitude indicates
218 that the former underestimates by about 50% the aerosol concentration in the range 0.4-1.0 μm (the
219 accuracy of the GRIMM has been verified by optical closure study against simultaneous aircraft
220 nephelometer measurements). This is estimated to induce a $\sim 20\%$ underestimation of the dN_{Acc}

221 calculated here. Conversely, the PCASP underestimation in the 0.4-1.0 μm range has almost a
222 negligible impact on $\text{dN}_{\text{Aitken}}$.

223 CPC measurements, and so $\text{dN}_{\text{Aitken}}$ data, were not available during SAFMED flights V49, V50, and
224 part of V51.

225

226 **3.3 Trace gases**

227 Carbon monoxide (CO) and ozone (O_3) mixing ratios were measured by the MOZART instrument
228 described in detail by Nedélec et al. (2003). CO is a long-lived tracer for air masses influenced by
229 combustion processes, whereas O_3 in the troposphere is a photochemical product of the oxidation of
230 CO and volatile organic compounds (VOCs) in the presence of nitrogen oxides (NO_x). CO and O_3
231 are measured at a resolution of 30 s and 4 s, respectively. The nominal uncertainty is $\pm 5\%$ for CO
232 and $\pm 2\%$ for O_3 (Nedélec et al., 2003). However, a recent airborne intercomparison in May 2014 in
233 the framework of the French ChemCallInt project and the TGOE European Joint Research Activity
234 has suggested a greater uncertainty (up to 30%) on CO measurement by MOZART on-board the
235 ATR-42 (A. Borbon, personal communication, 2015). Trace gas analysis will focus mostly on the
236 vertical distribution of the $\Delta\text{O}_3/\Delta\text{CO}$ ratio rather than absolute concentrations (see section 5.3) and
237 the uncertainty on CO should not affect data interpretation.

238

239 **3.4 STP conversion**

240 In order to compare measurements obtained at different altitudes the data presented here are
241 reported at standard temperature and pressure (STP) using $T=293.15$ K and $p=1013.25$ hPa (NIST,
242 National Institute of Standards and Technology, values). Hence, the scattering coefficient is scaled
243 to STP conditions and the particle concentrations are given as particles per standard cm^{-3} (scm^{-3}).

244 For a generic parameter x measured at the temperature T and pressure p , the conversion at STP is
245 calculated with the formula:

$$246 \quad x(\text{STP}) = x(T, p) \frac{T}{293.15} \frac{1013.25}{p} \quad (1).$$

247 CO and O₃ do not need to be corrected for STP since the mixing ratio does not depend on
248 temperature and pressure.

249

250 **3.5 Meteorological parameters**

251 The vertical profiles of the pressure (p), the temperature (T), the relative humidity (RH) and the
252 wind components towards the east and the north (U , V) measured on board the ATR-42 have been
253 used to analyse the atmospheric structure during flights. Starting from the measured parameters the
254 potential temperature (θ) has been also calculated as $\theta = T(p_0/p)^{0.286}$ with $p_0=1013.2$ mbar. For
255 each profile the height of the marine aerosol boundary layer (MABL) and planetary boundary layer
256 (BL) has been estimated visually by looking at the vertical gradients of T , θ , and RH.
257 Meteorological parameters have been also used to calculate the vertical profiles of the gradient
258 Richardson number (Ri):

$$259 \quad \text{Ri} = \frac{g}{\theta} \frac{\partial \theta}{\partial z} / \left(\left(\frac{\partial U}{\partial z} \right)^2 + \left(\frac{\partial V}{\partial z} \right)^2 \right) \quad (2).$$

260 In Eq. (2) g is the gravitational acceleration and z is the height. The Ri number is the ratio between
261 the buoyancy force and the wind shear and it is used to indicate dynamic stability and the formation
262 of clear air turbulence. Turbulence can develop when Ri is below the critical threshold $\text{Ri}_{\text{crit}}=0.25$,
263 while it is inhibited for $\text{Ri}>1$ (e.g., Wallace and Hobbs, 2006). In this study the profiles of Ri are

264 used to provide indications of favorable/unfavorable conditions for the development of turbulent
265 conditions within the atmosphere.

266

267 **3.6 Tracking the air mass back-trajectories**

268 The Lagrangian trajectory model FLEXTRA (FLEXible TRAjectories, Stohl et al., 1995) has been
269 used in selected cases to track the origin of sampled air masses. Five days three-dimensional back-
270 trajectories have been calculated using the ECMWF (European Centre for Medium-Range Weather
271 Forecast) operational analysis with a 0.5° by 0.5° horizontal resolution and up to 30 vertical model
272 levels below 4000 m. The model specific humidity and potential vorticity is also interpolated along
273 the trajectory path.

274

275 **4. Meteorological conditions, aerosol load, and pollution export regimes**

276 In order to characterize the general aerosol conditions encountered over the Western Mediterranean
277 basin during the TRAQA and the SAFMED campaigns we have plotted the time-series of the
278 aerosol optical depth (τ , ± 0.02) at 440 nm and the 440-870 nm Ångström exponent (α) measured
279 with a Cimel sunphotometer (Holben et al., 1998) at the three AERONET stations of Barcelona,
280 Frioul, and Ersal located along the coast around the Western basin (see Fig. 1). Level 1.5 cloud-
281 screened data are used in this study. Data are shown in Fig. 2 and correspond to the period of the
282 campaign of measurements plus 10 days before and after. Table 1 reports the date, location, and
283 main meteorological and export conditions encountered during TRAQA and SAFMED flights.

284 Over the analysed AERONET sites the aerosol optical depth was below 0.2 before the beginning of
285 the TRAQA campaign and increased, especially at Barcelona and Ersal, to ~ 0.3 - 0.5 (with $1 < \alpha < 2$) in
286 the periods 23-26 June and 3-13 July 2012. Isolated peaks of τ were measured in correspondence of
287 two Saharan dust intrusion events which occurred on the 17-23 June ($\tau \sim 0.6$) and 29 June 2012

288 ($\tau \sim 1.4$). Different wind regimes occurred during TRAQA and favoured the continental outflow
289 from different regions located around the basin. Two examples of wind maps derived from WRF-
290 Chem model (Grell et al., 2005) at 925 mbar are shown in Fig. 3 for 26 June and 3 July 2012. Main
291 observed meteorological/export conditions can be summarized as follows: (i) on 26-27 June
292 north/north-westerly winds blew across northern Italy determining an air mass outflow towards the
293 Gulf of Genoa (measurements on flights ~~V18~~-V19-V21); (ii) on the same days a strong Mistral-
294 Tramontane episode (i.e., strong northerly winds developing along the Rhône and Aude valley
295 which bring a northerly/north-westerly flow over the Western Mediterranean, see Fig 3a) favoured
296 the dispersion of pollutants towards the central part of the Western basin. Measurements during the
297 event were performed during flight V20; (iii) on 3-4 July the wind regime was dominated by
298 westerly/south-westerly winds mostly blowing at the surface across the Iberian Peninsula and
299 southwestern France (see Fig. 3b). This condition allowed measuring the export of pollution from
300 the Spanish coasts, in particular close to the area of Barcelona (flights V24-V25-V26, see Fig. 1).
301 Additionally, flight V31 sounded the atmospheric structure close to the Spanish coasts reaching the
302 southern urban area of Valencia. The flight was performed one week later (10 July) under a similar
303 meteorological condition characterized by~~the influence of~~ south-westerly winds favouring the
304 export from the Iberian Peninsula towards the basin; (iv) Mistral episodes occurred on the 6-7 and
305 11 July 2012. In those cases the Mistral wind combined with a persistent westerly flow thus
306 yielding pollution export towards the central and central-eastern part of the Western basin, as
307 measured during flights V27-V28-V30-V32; (v) finally, Saharan dust aerosols were sampled during
308 flights V16 and V20 (episode of the 17-23 June) and flights V22 and V23 (episode of the 29 June).
309 During SAFMED the meteorological conditions were more stable and two distinct phases were
310 observed: (i) a stable anticyclone affected the whole Western Mediterranean area during the first
311 half of July until the 26th, thus possibly favouring a more pronounced accumulation of
312 photochemical pollution in this part of the basin. Relatively high values of both τ ($\sim 0.2-0.8$) and α

313 (~1-2.5) were measured at the three sites of Barcelona, Frioul, and Erso in this period; (ii) a
314 cyclonic system moving from the Atlantic region towards Europe then affected the Western basin
315 on 28-29 July 2013. Very clean conditions ($\tau < 0.1-0.2$) were measured afterwards over the entire
316 region until the end of the SAFMED campaign. Winds were mostly westerly/south-westerly in the
317 first period of the campaign (24-29 July 2013, flights V46, V47, V48, V49, V50), which means that
318 the sampled air flow came mostly from the sea. Then, from 30 July to 1 August 2013 a north-
319 easterly flow affected the SAFMED investigated area thus promoting the export of pollution from
320 Northern Italy towards the Gulf of Genoa (flights V51, V52). A strong Mistral event (29 July-1
321 August) and two Saharan dust outbreaks (27-28 July and 1 August) affected the Western basin,
322 however not influencing the vertical profile observations during SAFMED.

323 In order to identify the distribution of observations during TRAQA and SAFMED as a function of
324 the aerosol type we have plotted in Figure 4 the distribution of the measured scattering coefficient
325 σ_s at 450, 550, and 700 nm as a function of the calculated scattering Ångström exponent α_s for all
326 vertical profiles. The plot shows a similar scattering intensity between cases dominated by coarse
327 particles ($\alpha_s < 0.5-1.0$), such as desert dust, and those dominated by fine particles ($\alpha_s > 1.0-1.5$), such
328 as pollution aerosols. For both dust and pollution σ_s peaks at about $100-120 \text{ Mm}^{-1}$. The frequency of
329 occurrence of α_s shows that pollution plumes represent the large majority of the cases observed,
330 with more than 70% of measurements with $\alpha_s > 1.0$.

331

332 5. Results

333 Figure 5 shows the box and whisker plots of the aerosol scattering coefficient σ_s at 450, 550, and
334 700 nm, particle number concentration in the Aitken (dN_{Aitken}) and accumulation (dN_{Acc}) diameter
335 ranges, and CO and O₃ measured in the boundary layer (BL) and in the free troposphere (FT) within
336 pollution plumes for all the different vertical soundings analysed in this study. This plot summarizes
337 the range of values observed during TRAQA and SAFMED. On average, the scattering coefficient

338 and CO are larger in the BL compared to the FT, whilst similar ranges of values are measured in the
339 two regions for dN_{Aitken} , dN_{Acc} , and O_3 . Even within the single BL and FT the different parameters
340 show a large variability that will be explored in the following paragraphs.

341

342 **5.1 Vertical profiles of aerosol concentration and scattering coefficient**

343 Figure 6 shows the vertical profiles of σ_s , dN_{Acc} , and dN_{Coarse} during TRAQA and SAFMED flights.
344 The date, time and coordinates of each profile, as well as the heights of the top of the marine and
345 planetary boundary layer (MABL and BL) estimated from meteorological data are also indicated in
346 the plot.

347 For the different vertical soundings the particle concentrations dN_{Acc} and dN_{Coarse} vary in the range
348 $\sim 30\text{-}3200 \text{ scm}^{-3}$ and $\sim 0.05\text{-}4000 \text{ scm}^{-3}$, respectively, for plumes with σ_s between 10 and 120 Mm^{-1} .
349 The structure in the scattering profile is generally mirrored in dN_{Acc} profile, and this also reflects the
350 pronounced spectral variability (i.e., decrease for increasing wavelength) of the scattering
351 coefficient, typical of pollution/anthropogenic particles. dN_{Coarse} also contributes to the scattering
352 signal in some cases especially at high altitudes (see V16, V20, V21, V22, and V23 above ~ 2000
353 m), and this reflects the low spectral variability of the scattering coefficient. These observations are
354 associated to the dust intrusion episodes which occurred in the Western Mediterranean basin during
355 TRAQA, which however will not be analysed in detail here. Aerosol layers affected by dust have
356 been labelled with a “D” in Fig. 6.

357 Maxima of the scattering coefficient have been measured for TRAQA flights V21 and V23 (~ 120
358 Mm^{-1} for pollution in the BL and $\sim 100 \text{ Mm}^{-1}$ in the dust layer), whereas flights V46-V48-V49,
359 during the first and more polluted phase of SAFMED, are the richest in dN_{Acc} ($1500\text{-}3000 \text{ scm}^{-3}$
360 over the whole column). Minima of σ_s and dN_{Acc} are obtained for flight V51 at the beginning of the
361 second SAFMED phase when clean conditions were observed in the Western Mediterranean.

362 Pollution plumes observed in the different flights extend from the boundary layer to the free
363 troposphere up to 3000-4000 m altitude. The vertical structure of the aerosol scattering
364 coefficient/particle concentration is linked to the variability of the atmospheric thermodynamic
365 structure and is generally characterized by a first layer confined in the MABL (<400 m, profiles
366 V16, V20, V22, V25, V48, V51), followed by one or more layers within the BL. In the FT pollution
367 particles occur both as single isolated plumes each about 500-1000 m deep (V21, V24, V25, V30,
368 V46, V49), or as a more uniform layer extending from the top of the BL up to 2500-4000 m altitude
369 (V26, V27, V28, V32, V48). The highest values of both the scattering coefficient and dN_{Acc} for
370 pollution are found within the MABL or BL in most cases, while a local minimum of σ_s and dN_{Acc}
371 is generally identified at the top of the BL. The scattering coefficient and the particle concentration
372 measured in the FT are comparable with the values observed in the BL, and in few cases even larger
373 (V25, V26, V30). Only in one case (profile V31) σ_s and dN_{Acc} decrease monotonically with height.
374 The aerosol vertical distribution, both in the BL and in the FT, often presents a strongly stratified
375 structure characterized by the presence of several thin sub-layers within one main identified aerosol
376 plume, as it can be seen in particular in the dN_{Acc} profiles (V20, V21, V22, V25, V46, V49).

377 The particle concentration in the Aitken mode (0.004-0.1 μm ; dN_{Aitken} , not shown in Fig. 6) is
378 generally below 5000-6000 scm^{-3} at all altitudes up to 4000 m within pollution plumes. dN_{Aitken} is
379 correlated with dN_{Acc} in most of the observed cases, which indicates the common source of particles
380 in these two size ranges. Few layers exceeding $\sim 10000\text{-}15000 \text{ scm}^{-3}$ are observed occasionally both
381 in the BL and in the FT. These will be discussed in more detail in Sect. 5.4.

382 The dN_{Acc} and dN_{Aitken} measurements within the BL and in the FT over the sea are comparable with
383 the values measured close to the surface at continental sites under pollution conditions (see Table 2)
384 (Petzold et al., 2002; Mallet et al., 2003 and 2005; Wiegner et al., 2006; Junkermann, 2009;
385 Hamburger et al., 2012; Highwood et al., 2012). This suggests that the export towards the basin
386 favours the redistribution of the pollution plumes along the vertical. Because of mixing in the BL,

387 measured concentrations within the BL can be as high as those observed close to the surface over
388 the continents. Values of dN as high as in the BL are observed in the FT because of transport in
389 specific conditions, as discussed below.

390 The observations of aerosol profiles obtained during TRAQA and SAFMED are representative of
391 the complex transport regimes which characterizes the export towards the Western basin and that is
392 mostly determined by the interaction between regional meteorology and local dynamics (e.g.,
393 Gangoiti et al., 2001). A first example is associated to the measurements in the area of Barcelona.
394 As discussed in Pérez et al. (2004) the presence of mountains up to ~500-3000 m altitude a few
395 kilometres inland favours, during summertime, the recirculation of pollutants along the coasts of
396 Spain. In these cases, the aerosols emitted at the surface in coastal areas are transported inland and
397 uplifted by sea breezes and mountain winds then the plumes are re-injected at different altitudes and
398 distances from the coast. During the TRAQA flights V24, V25, and V26, under the influence of
399 pollution outflow from the Barcelona area, we detected the presence of aerosol layers with elevated
400 concentrations ($dN_{Acc} \sim 2000-3000 \text{ scm}^{-3}$) up to 3500 m altitude at a distance of ~30 to 250 km from
401 the coast of Spain. Another example of complex dynamics linked to coastal orography is that
402 associated to the export from northern Italy and the Po Valley towards the Gulf of Genoa. The
403 presence of the Apennine Mountains close to the Ligurian coasts (max elevation ~1500-2000 m)
404 causes the uplift of continental air masses so determining the injection of aerosol plumes at different
405 altitudes both inside and outside the BL. Examples are given by flights V19, V21 and V52 for
406 which pollution aerosols from northern Italy are measured up to ~2000-3000 m altitude throughout
407 the Gulf of Genoa. Finally, another meteorological condition which largely influences the aerosol
408 export and distribution over the Western Mediterranean is the Mistral/Tramontane wind regime.
409 Under the influence of the Mistral flow, atmospheric aerosols can be dispersed as far as hundreds of
410 kilometres over the open sea, as discussed by Salameh et al. (2007). Examples are given in profiles

411 V20 and V28, performed at more than 100 km from the French coasts, for which pollution layers
412 associated to a Mistral flow are measured up to 2000-3000 m altitude.

413

414 **5.2 Trace gases vertical profiles**

415 Figure 7 shows O₃ versus CO for all TRAQA and SAFMED flights, while examples of CO and O₃
416 profiles representatives of different conditions are reported in Fig. 8 and 10.

417 CO and O₃ vary in the range 60-165 ppbv and 30-85 ppbv, respectively. The 25th and 75th
418 percentiles are 87 and 105 ppbv for CO and 49 and 62 ppbv for O₃, representative of moderate
419 pollution conditions (i.e., Parrish et al., 1998). By comparison, the values measured over land in
420 central Italy during flight V49 are in the range 80-180 ppbv for carbone monoxide and 40-85 ppbv
421 for ozone. CO and O₃ are generally correlated (correlation coefficient $R^2 \sim 0.5-0.8$) within measured
422 pollution plumes, and also correlated with σ_s and N_{Acc} both in the BL and in the FT, which indicates
423 photochemically active plumes. CO is generally higher in the BL, and shows absolute maxima in
424 the lowest levels (V20, V21, V24, V28, V46), then it decreases in the FT. Ozone presents a more
425 complicated vertical structure due to the different photochemical and dynamical processes which
426 control its formation and distribution. At first, local peaks of O₃ correlated with CO are observed in
427 correspondence of pollution plumes both in the BL and in the FT. An absolute maximum of O₃ is
428 sometimes found near the top of the BL (V24, V25, V30) possibly due to aged air masses trapped in
429 the boundary layer. Isolated peaks of O₃ (~75-80 ppbv) not correlated with aerosols and CO are also
430 measured in few cases above 3000-3500 m (V21, V25, V27, V28, V52). The analysis of back-
431 trajectories indicates that these high-altitude ozone layers are associated to the descent of air masses
432 travelling at about 7-8 km, which thus may suggest a downward transport from the upper
433 troposphere or the tropopause region due to a stratosphere-troposphere exchange (Ancellet and
434 Ravetta, 2005). Finally, absolute minima of O₃ (~15-30 ppbv) are measured within the dust layers

435 during flights V20 and V21, maybe related to the dust/ozone heterogeneous reactions which leads
436 to O₃ destruction, as documented in several studies (Bonasoni et al., 2004; Haywood et al., 2011).

437

438 **5.3 $\Delta O_3/\Delta CO$ and dN_{Aitken}/dN_{Acc} ratios and variability of pollution plume composition**

439 Using the O₃, CO, dN_{Aitken} and dN_{Acc} measurements we have estimated:

440 - the O₃-CO enhancement ratio ($\Delta O_3/\Delta CO$), i.e. the ratio of the ozone to carbon monoxide
441 variations compared to their baseline values. The $\Delta O_3/\Delta CO$ enhancement ratio is frequently
442 used to estimate the efficiency of O₃ formation and its export (Parrish et al., 1993; Zhang et
443 al., 2006). From our observations (Fig. 7) we have estimated a background value of ~70
444 ppbv in the BL and 60 ppbv in the FT for CO and ~30 ppbv for O₃ both in the BL and in the
445 FT.

446 - The Aitken to accumulation number ratio (dN_{Aitken}/dN_{Acc}), which defines the relative
447 importance of particles in the Aitken and accumulation modes. dN_{Aitken} is generally
448 associated to gas-to-particle conversion and nucleation events and is higher in fresh plumes,
449 while it decreases with the increasing of the plume lifetime due to coagulation or
450 condensation of water-soluble chemical species on the particle surface (Kulmala et al.,
451 2004).

452 The combination of $\Delta O_3/\Delta CO$ and dN_{Aitken}/dN_{Acc} has been used to retrieve additional information
453 on the atmospheric vertical structure, layering, and particle aging.

454 Within detected pollution plumes the ΔCO and ΔO_3 reach up to 100-120 ppbv and 45-55 ppbv,
455 respectively, with a corresponding $\Delta O_3/\Delta CO$ ratio which varies in the range ~0.10-2.0 for all cases.

456 The $\Delta O_3/\Delta CO$ ratio is highly noisy and this is due in part to the noise in the CO data, and in part
457 also possibly associated to the slight mismatch between CO and O₃ caused by their different time
458 resolution (30 s for CO and 4 s for O₃). These values of $\Delta O_3/\Delta CO$ obtained in this study are

Mis en forme : Non Surlignage

459 comparable with the range of observations available in the literature for fresh and moderately aged
460 pollution plumes in the BL and in the lower FT (~0.2-1.0) (Chin et al., 1994; Parrish et al., 1998;
461 Zhang et al., 2006; Cristofanelli et al., 2013). $dN_{\text{Aitken}}/dN_{\text{Acc}}$ is between about 1 and 20 in most of
462 pollution cases, which indicates the presence of both fresh layers rich in Aitken particles and aged
463 plumes poor in Aitken particles. Extremely high values of $dN_{\text{Aitken}}/dN_{\text{Acc}}$ (~50-200) are measured in
464 few cases in layers with very low dN_{Acc} concentrations.

465 The large variability in $\Delta O_3/\Delta CO$ and $dN_{\text{Aitken}}/dN_{\text{Acc}}$ indicates a strong heterogeneity in terms of
466 composition and lifetime for the different observed plumes. This heterogeneity reflects the
467 complexity in terms of sources, production processes, and transport mechanisms which
468 characterizes the Western basin. In order to illustrate this point, we have selected three examples
469 representative of different conditions observed in different areas of the basin: (i) V19, performed in
470 the Gulf of Genoa in correspondence of continental outflow events from Northern Italy/Po Valley;
471 (ii) V20, performed in Southern France during a Mistral event; (iii) V24, which measured the export
472 of pollution from the area of Barcelona. The vertical profiles of the spectral scattering coefficient σ_s ,
473 temperature T, relative humidity RH, dN_{Acc} , dN_{Aitken} , CO, O₃, $\Delta O_3/\Delta CO$, $dN_{\text{Aitken}}/dN_{\text{Acc}}$ and wind
474 are reported in Fig. 8 for these cases.

475 *1. V19: export from northern Italy/Po Valley.* The profile shown for flight V19 (Fig. 8a) is
476 characterized by the presence of three different aerosol structures: the first one below 800 m,
477 characterized by a lower $dN_{\text{Aitken}}/dN_{\text{Acc}}$ (~1-5) and relatively high $\Delta O_3/\Delta CO$ (~0.4-1.5), possibly
478 associated to moderately aged pollution; the second one between 800 and 2600 m, richer in fine
479 particles ($dN_{\text{Aitken}}/dN_{\text{Acc}}$ ~5-15), so possibly linked to fresher emissions; and the third one above
480 2600 m, where the ratio $dN_{\text{Aitken}}/dN_{\text{Acc}}$ rises rapidly, as will be further discussed in Sect. 5.4. The
481 export of fresh pollution at 800-2600 m from northern Italy as observed in V19 may be related to
482 the peculiar orography of this region and the uplift of continental air masses. This is confirmed by
483 the analysis of the back-trajectories (Fig. 9) which indicates that the air masses arriving at 1000 and

484 2000 m passed over the western Po Valley at an altitude of about 400-1200 m and were then
485 uplifted near the Ligurian coast to enter the basin above the BL. Junkermann (2009) measured high
486 levels of fine particles up to about 2000 m in the western Po Valley, which means that the altitudes
487 of 400-1200 m reached by our investigated air masses could have been sufficient for them to collect
488 fresh emitted particles along their path. Conversely, below 800 m the air mass trajectory shows a
489 longer subsidence over the sea surface in the troposphere which has possibly favoured the advection
490 of more aged plumes, or the mixing with sea salts thus inducing the decrease of the $dN_{\text{Aitken}}/dN_{\text{Acc}}$
491 ratio. It should be noted that the aerosol layer in the FT also shows relatively higher values of the
492 $\Delta O_3/\Delta CO$ ratio ($\sim 0.6-1.0$) compared to the more aged plume in the BL. The enhanced amount of O_3
493 in this air mass can be linked to a high concentration of volatile precursors which may have
494 favoured the build-up of ozone during the plume evolution. In a recent work, Kaiser et al. (2014)
495 suggest that in the Po Valley the high content of formaldehyde, also observed by Junkermann et al.
496 (2009), may be responsible for the excess of O_3 production. Fresh layers in the FT up to $\sim 2000-$
497 3000 m possibly associated to pollution export from northern Italy have been also observed during
498 flights V21 and V52 (not shown).

499 *2. V20: export during a Mistral/Tramontane event.* V20 provides an example of export during a
500 Mistral/Tramontane event. As shown in Fig. 8b, winds from the northwest direction are measured at
501 all altitudes during flight V20. The aerosol profile in the BL is characterized in the first ~ 400 m by
502 the presence of a layer richer in dN_{Aitken} ($dN_{\text{Aitken}}/dN_{\text{Acc}} > 20$) and CO (100 ppbv close to the surface;
503 CO data not available between 150 and 650 m) possibly linked to fresh pollution, followed by the
504 alternation of several layers characterized by a variable dN_{Aitken} ($1000-6000 \text{ scm}^{-3}$) and lower CO
505 (~ 70 ppbv). A local minimum of dN_{Aitken} and σ_s is found at ~ 400 m. For all these layers the O_3 is
506 very low ($\sim 30-40$ ppbv) and the $\Delta O_3/\Delta CO$ ratio is $< 0.6-0.8$. At higher altitudes, between 1400 and
507 2000 m, we observe a layer enriched in O_3 ($\Delta O_3/\Delta CO \sim 1-2$) in correspondence of an almost aerosol-
508 free region. This enriched ozone layer might be possibly associated to a downward transport from

509 higher tropospheric layers, as also suggested by the back-trajectories (Fig. 9), as well as to the
510 mixing with ozone rich layers along the air mass trajectory. Larger particles, from long-range
511 transport of Saharan dust at latitudes below 30° N, are measured between 2000 and 3000 m, with a
512 minimum of O₃ (~15-20 ppbv) registered within the layer. Several other flights were performed
513 during Mistral/Tramontane episodes (V27, V28, V30, V32) and show, similarly to V20, the
514 presence of several layers both in the BL and the FT.

515 *3. V24: export from the Barcelona area.* Measurements during V24 may be taken as representative
516 of local recirculation (Pérez et al., 2004). In the V24 profile in Fig. 8c we may recognize up to 5
517 different aerosol layers. A first layer at <200 m within the MABL, coming from the southwest and
518 directly exported from the area of Barcelona. The layer is characterized by high CO (90-120 ppbv),
519 and relatively low values of dN_{Aitken} (~4000 scm⁻³) and O₃ (~50 ppbv), which possibly suggest the
520 mixing of pollution with marine particles close to the sea surface. A second layer of fresher
521 particles, always coming from the southwestern direction, is observed above the MABL between
522 200 and 600 m (dN_{Aitken}~6000-8000 scm⁻³, O₃~70 ppb, with dN_{Aitken}/dN_{Acc}~5-15, and
523 ΔO₃/ΔCO~0.8-1.5). A third, more aged, sublayer (dN_{Aitken}/dN_{Acc}~2-5, ΔO₃/ΔCO~0.8-1.0) is
524 observed within the BL between 600 and 1000 m. The FT is characterized by the presence of
525 moderately aged plumes from ~1000 to 2800 m (dN_{Aitken}/dN_{Acc}~2-10, ΔO₃/ΔCO~0.2-0.8), and a
526 very aged plume at 2800-3800 m almost deprived in Aitken particles and richer in O₃
527 (dN_{Aitken}/dN_{Acc}<1, ΔO₃/ΔCO~0.6-1.5). A marked local minimum is observed at the top of the BL
528 for σ_s, dN_{Acc}, dN_{Aitken}, CO, and O₃, suggesting the presence of air masses with different origin
529 between the BL and the FT. This is also confirmed by the analysis of the back-trajectories (Fig. 9)
530 which indicates a low level air masses coming from the Spanish coasts in the BL, and air masses
531 travelling at higher altitudes in the FT. In particular, the layer at 2800-3800 m is possibly associated
532 to an intercontinental transport from Northern America, as shown in the trajectory ending at 3500

533 m. A similar structure characterized by the alternation of fresher and more aged plumes in the BL
534 and FT is also observed in V25 for which aerosol layers are detected up to 4000 m altitude.

535 The detailed analysis of these three events evidences the complexity of the atmospheric structure
536 over the Western Mediterranean basin in link with the different dynamical processes involved.

537

538 **5.4 Layers with enhanced Aitken mode particle numbers**

539 Isolated layers with $dN_{\text{Aitken}} \sim 10000\text{-}15000 \text{ scm}^{-3}$ have been observed occasionally both in the BL
540 and in the FT. The vertical profiles of dN_{Aitken} for some selected cases are shown in Fig. 10.

541 For about half of the observed events the dN_{Aitken} layer appears related to a simultaneous increase in
542 dN_{Acc} , CO, and O₃, which suggests that the layer has been transported from a region directly
543 emitting in this size range. These cases are: V16 at ~200-400 m, V21 at ~400-800 m, V28 at ~250
544 m, and V31 at ~1000-3000 m (only V28 and V31 are shown in Fig. 10). The most remarkable
545 example is V31 (Fig. 10a), performed close to the coasts of Spain near Valencia, for which the high
546 dN_{Aitken} layer extends from the top of the BL to ~3000 m altitude. The wind vector and the back-
547 trajectories (not shown) indicates that the air mass comes from the western-southwestern direction
548 above 1000 m, so the dN_{Aitken} layer can be directly related to pollution export from the urban region
549 of Valencia.

550 In all the other cases the high dN_{Aitken} layer is generally not related to simultaneous dN_{Acc} and O₃
551 increase. Two of these cases (V16 at ~800-1000 m and V28 at ~100 m) occur in the BL.

552 For the V28 layer (Fig. 10b) the dN_{Aitken} is correlated with CO which might indicate the influence of
553 local emissions close to the surface level (i.e., ship emissions). CO values are relatively high (140-
554 160 ppbv) within the layer. It has been often assumed that new particle formation events (NPF) only
555 occur in almost clean environments (e.g., O'Dowd et al., 2010; Sellegri et al., 2010), and that they
556 are suppressed under polluted conditions. In a recent study, Brines et al. (2014) show the occurrence

557 of NPF events also in urban areas with high level of pollution in the Mediterranean region. So, we
558 explore the possibility of NPF in our observations. Given the size ranges of the CPC and PCASP,
559 however, we cannot discriminate within dN_{Aitken} the particle concentration in the sole 4-20 nm
560 range, i.e. the size range involved in nucleation. So it is not possible to directly associate the V28
561 observations to NPF. In order to obtain a qualitative indication of the possible occurrence of NPF,
562 we have looked at the air mass dynamics within the layer. Several studies suggest, in fact, that NPF
563 might be favoured by turbulence and air mass mixing (e.g., Nilsson et al., 2001; Wehner et al.,
564 2010). We have thus looked at the gradient Richardson number (Ri) which gives information on the
565 atmospheric dynamical stability. Vertical profiles of Ri are also shown in Fig. 10. For V28 the
566 vertical profile of Ri indicates that below 200 m the Ri number is consistently below zero, which
567 suggests well established turbulent conditions possibly favouring NPF in this layer.

568 In other two cases (V19, Fig. 10c, and V26, Fig. 10d), under lower pollution conditions ($\text{CO} < 100$),
569 we measured high dN_{Aitken} concentration in correspondence of low dN_{Acc} layers in the FT at ~2800-
570 3000 m for V19 and 3500-4500 m for V26. For V19 and V26 layers, dN_{Aitken} seems anticorrelated
571 to CO. Also in this case the Richardson number is below Ri_{crit} in correspondence of the Aitken peak
572 meaning that conditions are favorable for turbulence within the layer, and this may indicate also in
573 this case the possible role of NPF.

574 Finally, a case of high dN_{Aitken} concentration has been also observed in correspondence of dust
575 particles between ~3000 and 4000 m (V23b, Fig. 10e). This layer can be possibly linked to the
576 photochemically-induced nucleation which may occur in presence of dust and SO_2 as hypothesised
577 in a recent study by Dupart et al. (2012) and observed by Nie et al. (2014).

578

579 **6. Conclusions**

580 The data presented in this paper gives an overview of the distribution of aerosols and trace gases
581 within the tropospheric column up to 5000 m above the Western Mediterranean basin.

582 These data add to the very few available measurements of aerosol and trace gases vertical profiles
583 over the sea surface in the Central (e.g., Junkermann, 2001; Meloni et al., 2003; Di Iorio et al.,
584 2003; Pace et al., 2014) and Eastern (e.g., Formenti et al., 2002; Dulac and Chazette, 2003) parts of
585 the basin thus contributing to improve the description of the atmospheric composition and structure
586 over the whole Mediterranean area.

587 Observations from the present study indicate that continental pollution strongly affects the
588 composition and structure of the Western Mediterranean basin both close to coastal regions and in
589 the open sea. Pollution layers extend up to 250 km far from the coasts and reach up to 3000-4000 m
590 altitude, presenting a complex and highly stratified structure. The measured particle concentration is
591 comparable with the values reported for continental Europe (Petzold et al., 2002; Junkermann,
592 2009; Hamburger et al., 2012).

593 Pollution plumes with different compositions, origins, and lifetimes are observed in link with the
594 different observed dynamical export conditions and meteorological regimes. The aerosol and trace
595 gas observations during TRAQA and SAFMED are consistent with the results of former campaigns
596 and with the interpretation of observed or well known air-masses dynamics and meteorological
597 phenomena that can occur in the Western basin (Flamant and Pelon, 1996; Millan et al., 1997;
598 Gangoiti et al., 2001; Pérez et al., 2004; Mallet et al., 2005).

599 The large heterogeneity in aerosol compositions, origins, and lifetimes as documented in this study
600 can reflect in a large heterogeneity of aerosol optical properties, with consequences for their direct
601 radiative effect in this part of the basin. This aspect will be investigated in a companion paper
602 analysing the TRAQA and SAFMED in situ measurements of the aerosol absorption and scattering
603 properties and their variability.

604 From the present observations, it is also interesting to note the relatively high values of dN_{Aitken}
605 measured both in the BL and the FT, which evidences the important contribution of ultrafine
606 particles at all altitudes over the basin. These can be linked to the different export mechanisms

607 previously discussed, as well as the possible occurrence of NPF events. Aitken particle profiles are
608 very rare over the sea surface in the Mediterranean (e.g., Junkermann et al. 2001; Pace et al., 2015)
609 and data comparison is quite difficult. Few studies have observed NPF in the FT in continental
610 areas (Boulon et al., 2010; Rose et al., 2014) and suggest that the export of pollution into the upper
611 troposphere, as it is common in the Western basin, might promote the occurrence of these events.
612 The observations of the present study may thus also have very large implications due to the crucial
613 role of NPF in controlling the atmospheric cloud condensation nuclei concentration (Spracklen et
614 al., 2008) and the associated aerosol indirect effect on climate.

615

616 **Author contributions**

617 J.-L.A., F.R., G.A., M.B., A.B., P.F. and K.S. designed the TRAQA and SAFMED experiments and
618 coordinated the campaigns. C.G., N.G., and C.D.B operated the instruments on board the ATR-42
619 during the flights. C.D.B. performed the data analysis with contributions from L.D., P.F., F.R.,
620 A.B., G.A., J.-C.R., and M.B.. G.A. performed the FLEXTRA simulations. J.-C.R. performed the
621 WRF-Chem simulations. C.D.B. wrote the manuscript.

622

623 **Acknowledgements**

624 All measurement presented here are from the Chemistry-Aerosol Mediterranean Experiment project
625 (ChArMEx, <http://charmex.lsce.ipsl.fr>), which is the atmospheric component of the French
626 multidisplinary program MISTRALS (Mediterranean Integrated Studies aT Regional And Local
627 Scales). ChArMEx-France was principally funded by INSU, ADEME, ANR, CNES, CTC (Corsica
628 region), EU/FEDER, Météo-France, and CEA. TRAQA was funded by ADEME/PRIMEQUAL and
629 MISTRALS/ChArMEx programmes and Observatoire Midi-Pyrénées. SAFMED was funded by the
630 ANR project SAF-MED (Secondary Aerosol Formation in the MEDiterranean, grant SIMI6 ANR-

631 12-BS06-0013). C. Di Biagio thanks the Centre National des Etudes Spatiales (CNES) for financial
632 support.

633 The authors wish to thank the technicians, pilots and ground crew of SAFIRE (Service des Avions
634 Français Instruments pour la Recherche en Environnement) for facilitating the instrument
635 integration and conducting flying operations. We thank S. Chevaillier, L. Girault, R. Loislil, J.
636 Pelon, S. Triquet, and P. Zapf for their contribution during the campaigns. We thank S. Basart, J.
637 M. Baldasano, M. Mallet, P. Goloub, J. Piazzola and their staff for establishing and maintaining the
638 Barcelona, Ersu, and Frioul AERONET sites. Helpful discussions with G. Pace are gratefully
639 acknowledged. We thank also two anonymous reviewers whose suggestions helped to clarify the
640 manuscript.

641

642

643 **References**

- 644 Ancellet, G. and Ravetta, F.: Analysis and validation of ozone variability observed by lidar during
645 the ESCOMPTE-2001 campaign, *Atmos. Res.*, 74, 435–459, 2005.
- 646 Anderson, T. L., Covert, D. S., Marshall, S. F., Laucks, M. L., Charlson, R. J., Waggoner, A. P.,
647 Ogren, J. A., Caldow, R., Holm, R. L., Quant, F. R., Sem, G. J., Wiedensholer, A., Ahlquist, N.
648 A., and Bates, T. S.: Performance characteristics of a high-sensitivity, three-wavelength, total
649 scatter/backscatter nephelometer, *J. Atmos. Ocean. Tech.*, 13, 967–986, 1996.
- 650 Anderson, T. L. and Ogren, J. A.: Determining aerosol radiative properties using the TSI 3563
651 integrating nephelometer, *Aerosol Sci. Technol.*, 29, 57–69, 1998.
- 652 Bonasoni, P., Cristofanelli, P., Calzolari, F., Bonafè, U., Evangelisti, F., Stohl, A., Zauli Sajani, S.,
653 van Dingenen, R., Colombo, T., and Balkanski, Y.: Aerosol-ozone correlations during dust
654 transport episodes, *Atmos. Chem. Phys.*, 4, 1201-1215, doi:10.5194/acp-4-1201-2004, 2004.
- 655 Boucher, O., Randall, D., Artaxo, P., Bretherton, C., Feingold, G., Forster, P., Kerminen, V.-M.,
656 Kondo, Y., Liao, H., Lohmann, U., Rasch, P., Satheesh, S. K., Sherwood, S., Stevens, B., and
657 Zhang, X. Y.: Clouds and Aerosols. In: *Climate Change 2013: The Physical Science Basis.*
658 *Contribution of Working Group I to the Fifth Assessment Report of the Intergovernmental Panel*
659 *on Climate Change* [Stocker, T.F., D. Qin, G.-K. Plattner, M. Tignor, S.K. Allen, J. Boschung,
660 A. Nauels, Y. Xia, V. Bex and P.M. Midgley (eds.)]. Cambridge University Press, Cambridge,
661 United Kingdom and New York, NY, USA, 571-657, 2013.
- 662 Boulon, J., Sellegri, K., Venzac, H., Picard, D., Weingartner, E., Wehrle, G., Collaud Coen, M.,
663 Bütikofer, R., Flückiger, E., Baltensperger, U., and Laj, P.: New particle formation and ultrafine

664 charged aerosol climatology at a high altitude site in the Alps (Jungfraujoch, 3580 m a.s.l.,
665 Switzerland), *Atmos. Chem. Phys.*, 10, 9333–9349, doi: 10.5194/acp-10-9333-2010, 2010.

666 Brines, M., Dall'Osto, M., Beddows, D. C. S., Harrison, R. M., Gómez-Moreno, F., Núñez, L.,
667 Artíñano, B., Costabile, F., Gobbi, G. P., Salimi, F., Morawska, L., Sioutas, C., and Querol, X.:
668 Frequency of new particle formation events in the urban Mediterranean climate, *Atmos. Chem.*
669 *Phys. Discuss.*, 14, 26463-26494, doi:10.5194/acpd-14-26463-2014, 2014.

670 Chazette, P., Randriamiarisoa, H., Sanak, J., Couvert, P., and Flamant, C.: Optical properties of
671 urban aerosol from airborne and ground based in situ measurements performed during the
672 ESQUIF program, *J. Geophys. Res.*, 110, D02206, doi:10.1029/2004JD004810, 2005.

673 Chin, M., Jacob, D. J., Munger, J. W., Parrish, D. D., and Doddridge, B. G.: Relationship of ozone
674 and carbon monoxide over North America, *J. Geophys. Res.*, 99, 14,565–14,573, 1994.

675 Colette, A., Ancellet, G., Menut, L., and Arnold, S. R.: A Lagrangian analysis of the impact of
676 transport and transformation on the ozone stratification observed in the free troposphere during
677 the ESCOMPTE campaign, *Atmos. Chem. Phys.*, 6, 3487-3503, doi:10.5194/acp-6-3487-2006,
678 2006.

679 Cristofanelli, P., Fierli, F., Marinoni, A., Calzolari, F., Duchi, R., Burkhardt, J., Stohl, A., Maione,
680 M., Arduini, J., and Bonasoni, P.: Influence of biomass burning and anthropogenic emissions on
681 ozone, carbon monoxide and black carbon at the Mt. Cimone GAW-WMO global station (Italy,
682 2165 m a.s.l.), *Atmos. Chem. Phys.*, 13, 15–30, 2013.

683 Di Iorio, T., di Sarra, A., Junkermann, W., Cacciani, M., Fiocco, G., and Fua`, D.: Tropospheric
684 aerosols in the Mediterranean: 1. Microphysical and optical properties, *J. Geophys. Res.*,
685 108(D10), 4316, doi:10.1029/2002JD002815, 2003.

686 Drobinski, P, Saïd, F., Ancellet, G., Arteta, J. Augustin, P., Bastin, S., Brut, A., Caccia, J. L.,
687 Campistron, B., Cautenet, S., Colette, A., Coll, I., Corsmeier, U., Cros, B., Dabas, A., Delbarre,
688 H., Dufour, A., Durand, P., Guénard, V., Hasel, M., Kalthoff, N., Kottmeier, C., Lasry, F.,
689 Lemonsu, A., Lohou, F., Masson, V., Menut, L., Moppert, C., Peuch, V. H., Puygrenier, V.,
690 Reitebuch, O., and Vautard, R.: Regional transport and dilution during high-pollution episodes in
691 southern France: Summary of findings from the Field Experiment to Constraint Models of
692 Atmospheric Pollution and Emissions Transport (ESCOMPTE), *J. Geophys. Res.*, 112, D13105,
693 doi:10.1029/2006JD007494, 2007.

694 Dulac, F., and Chazette, P.: Airborne study of a multi-layer aerosol structure in the eastern
695 Mediterranean observed with the airborne polarized lidar ALEX during a STAAARTE campaign
696 (7 June 1997), *Atmos. Chem. Phys.*, 3, 1817-1831, doi:10.5194/acp-3-1817-2003, 2003.

697 Dupart, Y.; King, S. M., Nekat, B., Nowak, A., Wiedensohler, A., Herrmann, H., David, G.,
698 Thomas, B., Miffre, A., Rairoux, P., D'Anna, B., and George, C.: Mineral dust photochemistry
699 induces nucleation events in the presence of SO₂. *PNAS*, 109, (51), 20842–20847, 2012.

700 Ebert, M., Weinbruch, S., Rausch, A., Gorzawski, G., Hoffmann, P., Wex, H., and Helas, G.: The
701 complex refractive index of aerosols during LACE 98 as derived from the analysis of individual
702 particles, *J. Geophys. Res.*, 107, D21, 8121, doi:10.1029/2000JD000195, 2002.

703 Ebert, M., Weinbruch, S., Hoffmann, P., and Ortner, H. M.: The chemical composition and complex
704 refractive index of rural and urban influenced aerosols determined by individual particle
705 analysis, *Atmos. Environ.*, 38, 6531–6545, 2004.

706 Flamant, C., and Pelon, J.: Atmospheric boundary-layer structure over the Mediterranean during a
707 Tramontane event, *Quart. J. Roy. Meteorol. Soc.*, 122, 1741–1778, 1996.

708 Formenti, P., Reiner, T., Sprung, D., Andreae, M. O., Wendisch, M., Wex, H., Kindred, D., Dewey,
709 K., Kent, J., Tzortziou, M., Vasaras, A., and Zerefos, C.: STAAARTE-MED 1998 summer
710 airborne measurements over the Aegean Sea, 1, Aerosol particles and trace gases, *J. Geophys.*
711 *Res.*, 107, D21, doi:10.1029/2001JD001337, 2002.

712 Formenti, P., Rajot, J. L., Desboeufs, K., Saïd, F., Grand, N., Chevaillier, S., and Schmechtig, C.:
713 Airborne observations of mineral dust over western Africa in the summer Monsoon season:
714 spatial and vertical variability of physico-chemical and optical properties, *Atmos. Chem. Phys.*,
715 11, 6387–6410, doi:10.5194/acp-11-6387-2011, 2011.

716 Gangoiti, G., M. M. Millán, R. Salvador, E. Mantilla: Long-Range transport and recirculation of
717 pollutants in the Western Mediterranean during the RECAPMA Project. *Atmos. Environ.*, 35,
718 6267–6276, 2001.

719 Gkikas, A., Housos, E. E., Hatzianastassiou, N., Papadimas, C. D., and Bartzokas, A.: Synoptic
720 conditions favouring the occurrence of aerosol episodes over the broader Mediterranean basin,
721 *Q. J. R. Meteorol. Soc.*, 138: 932–949. doi:10.1002/qj.978, 2012.

722 Grell, G. A., Peckham, S. E., Schmitz, R., McKeen, S. A., Frost, G., Skamarock, W. C., and Eder,
723 B.: Fully coupled “online” chemistry within the WRF model, *Atmos. Environ.*, 39, 6957–6975,
724 2005.

725 Hamburger, T., McMeeking, G., Minikin, A., Petzold, A., Coe, H., and Krejci, R.: Airborne
726 observations of aerosol microphysical properties and particle ageing processes in the troposphere
727 above Europe, *Atmos. Chem. Phys.*, 12, 11533–11554, doi:10.5194/acp-12-11533-2012, 2012.

728 Haywood, J., Johnson, B., Osborne, S., Mulcahy, J., Brooks, M., Harrison, M., Milton, S., and
729 Brindley, H.: Observations and modelling of the solar and terrestrial radiative effects of Saharan
730 dust: a radiative closure case-study over oceans during the GERBILS campaign, *Q. J. R.*
731 *Meteorol. Soc.*, 137, 1211–1226, doi:10.1002/qj.770, 2011.

732 Highwood, E. J., Northway, M. J., McMeeking, G. R., Morgan, W. T., Liu, D., Osborne, S.,
733 Bower, K., Coe, H., Ryder, C., and Williams, P.: Aerosol scattering and absorption during the
734 EUCAARI-LONGREX flights of the Facility for Airborne Atmospheric Measurements (FAAM)
735 BAe-146: can measurements and models agree?, *Atmos. Chem. Phys.*, 12, 7251–7267,
736 doi:10.5194/acp-12-7251-2012, 2012.

737 Holben, B. N., Eck, T. F., Slutsker, I., Tanré, D., Buis, J. P., Setzer, A., Vermote, E., Reagan, J. A.,
738 Kaufman, Y., Nakajima, T., Lavenu, F., Jankowiak, I., and Smirnov, A.: AERONET: a federated
739 instrument network and data archive for aerosol characterization, *Rem. Sens. Environ.*, 66, 1–16,
740 1998.

741 Jiménez, P., Pérez, C., Rodríguez, A., and Baldasano, J. M. : Correlated levels of particulate matter
742 and ozone in the western Mediterranean basin: Air quality and lidar measurements, 22nd Annual
743 Conference Am. Assoc. for Aerosol Res., Anaheim, California, 20–24 October 20–24 2003,
744 2003.

745 Jiménez, P., Lelieveld, J., and Baldasano, J. M.: Multiscale modeling of air pollutants dynamics in
746 the northwestern Mediterranean basin during a typical summertime episode, *J. Geophys. Res.*,
747 111, D18306, doi:10.1029/2005JD006516, 2006.

748 Jiménez-Guerrero, P., Jorba, O., Baldasano, J. M., and Gassó, S.: The use of a modelling system as
749 a tool for air quality management: Annual high-resolution simulations and evaluation, *Sci. Tot.*
750 *Environ.*, 390, 323–340, 2008.

751 Junkermann, W.: An ultralight aircraft as platform for research in the lower troposphere: System
752 performance and first results from radiation transfer studies in stratiform aerosol layers and
753 broken cloud conditions, *J. Atmos. Oceanic Technol.*, 18, 934–946, 2001.

- 754 Junkermann, W.: On the distribution of formaldehyde in the western Po-Valley, Italy, during 800
755 FORMAT 2002/2003, *Atmos. Chem. Phys.*, 9, 9187-9196, doi:10.5194/acp-9-9187-2009, 2009.
- 756 Kaiser, J., Wolfe, G. M., Bohn, B., Broch, S., Fuchs, H., Ganzeveld, L. N., Gomm, S., Häsel, R.,
757 Hofzumahaus, A., Holland, F., Jäger, J., Li, X., Lohse, I., Lu, K., Rohrer, F., Wegener, R.,
758 Mentel, T. F., Kiendler-Scharr, A., Wahner, A., and Keutsch, F. N.: Evidence for an unidentified
759 ground-level source of formaldehyde in the Po Valley with potential implications for ozone
760 production, *Atmos. Chem. Phys. Discuss.*, 14, 25139-25165, doi:10.5194/acpd-14-25139-2014,
761 2014.
- 762 Kallos, G., Astitha, M., Katsafados, P., and Spyrou, C.: Long-range transport of anthropogenically
763 and naturally produced particulate matter in the Mediterranean and North Atlantic: Current state
764 of knowledge, *J. Appl. Meteorol. Climatol.*, 46, 1230–1251, 2007.
- 765 Kulmala, M., Vehkamäki, H., Petaja, T., Dal Maso, M., Lauri, A., Kerminen, V.-M., Birmili, W.,
766 and McMurry, P.H.: Formation and growth rates of ultrafine atmospheric particles: A review of
767 observations, *J. Aerosol Sci.*, 35(2), 143–176, 2004.
- 768 Lelieveld, J., Berresheim, H., Borrmann, S., Crutzen, P. J., Dentener, F. J., Fischer, H., Feichter, J.,
769 Flatau, P. J., Heland, J., Holzinger, R., Korrmann, R., Lawrence, M. G., Levin, Z., Markowicz,
770 K. M., Mihalopoulos, N., Minikin, A., Ramanathan, V., de Reus, M., Roelofs, G. J., Scheeren,
771 H. A., Sciare, J., Schlager, H., Schultz, M., Siegmund, P., Steil, B., Stephanou, E. G., Stier, P.,
772 Traub, M., Warneke, C., Williams, J., and Ziereis H.: Global air pollution crossroads over the
773 Mediterranean, *Science*, 298, 794–799, doi:10.1126/science.1075457, 2002.
- 774 Liu, Y. and Daum, P.: The effect of refractive index on size distributions and light scattering
775 coefficients derived from optical particle counters, *J. Aerosol Sci.*, 31, 945–957, 2000.
- 776 Mallet, M., Roger, J. C., Despiiau, S., Dubovik, O., and Putaud, J. P.: Microphysical and optical
777 properties of aerosol particles in urban zone during ESCOMPTE, *Atmos. Res.*, 69, 73–97, 15
778 2003.
- 779 Mallet, M., Van Dingenen, R., Roger, J. C., Despiiau, S., and Cachier, H.: In situ airborne
780 measurements of aerosol optical properties during photochemical pollution events, *J. Geophys.*
781 *Res.*, 110, D03205, doi:10.1029/2004JD005139, 2005.
- 782 Mallet, M., Gomes, L., Solmon, F., Sellegri, K., Pont, V., Roger, J. C., Missamou, T., and Piazzola,
783 J.: Calculation of key optical properties of the main anthropogenic aerosols over the Western
784 French coastal Mediterranean Sea, *Atmos. Res.*, 101, 396–411, 2011.
- 785 Meloni, D., di Sarra, A., DeLuigi, J., Di Iorio, T., Fiocco, G., Junkermann, W., and Pace, G.:
786 Tropospheric aerosols in the Mediterranean: 2. Radiative effects through model simulations and
787 measurements, *J. Geophys. Res.*, 108(D10), 4317, doi:10.1029/2002JD002807, 2003.
- 788 Millán, M., Salvador, R., Mantilla, E., and Artinãno, B.: Meteorology and photochemical air
789 pollution in Southern Europe: experimental results from EC research projects, *Atmos. Environ.*,
790 30 (12), 1909–1924, 1996.
- 791 Millan, M. M., Salvador, R., Mantilla, E., and Kallos, G.: Photooxidant dynamics in the Western
792 Mediterranean in summer: Results from European research projects, *J. Geophys. Res.*, 102(D7),
793 8811–8823, 1997.
- 794 Millán, M. M., Mantilla, E., Salvador, R., Carratala, A., Sanz, M. J., Alonso, L., Gangoiti, G., and
795 Navazo, M.: Ozone cycles in the western Mediterranean basin: interpretation of monitoring data
796 in complex terrain, *J. Appl. Meteorol.*, 4, 487–507, 2000.
- 797 Monks, P., Granier, C., Fuzzi, S., Stohl, A., Williams, M., Akimoto, H., Amann, M., Baklanov, A.,
798 Baltensperger, U., Bey, I., Blake, N., Blake, R., Carslaw, K., Cooper, O., Dentener, F., Fowler,

799 D., Fragkou, E., Frost, G., Generoso, S., Ginoux, P., Grewe, V., Guenther, A., Hansson, H.,
800 Henne, S., Hjorth, J., Hofzumahaus, A., Huntrieser, H., Isaksen, I., Jenkin, M., Kaiser, J.,
801 Kanakidou, M., Klimont, Z., Kulmala, M., Laj, P., Lawrence, M., Lee, J., Liousse, C., Maione,
802 M., McFiggans, G., Metzger, A., Mieville, A., Moussiopoulos, N., Orlando, J., O'Dowd, C.,
803 Palmer, P., Parrish, D., Petzold, A., Platt, U., Pöschl, U., Prévôt, A., Reeves, C., Reimann, S.,
804 Rudich, Y., Sellegri, K., Steinbrecher, R., Simpson, D., ten Brink, H., Theloke, J., van der Werf,
805 G., Vautard, R., Vestreng, V., Vlachokostas, C., and von Glasow, R.: Atmospheric composition
806 change – global and regional air quality, *Atmos. Environ.*, 43, 5268–5350,
807 doi:10.1016/j.atmosenv.2009.08.021, 2009.

808 Müller, D., Ansmann, A., Wagner, F., Franke, K., and Althausen, D.: European pollution outbreaks
809 during ACE 2: Microphysical particle properties and single-scattering albedo inferred from
810 multiwavelength lidar observations, *J. Geophys. Res.*, 107, D15, 4248, 10.1029/2001JD001110,
811 2002.

812 Nedélec, P., Cammas, J.-P., Thouret, V., Athier, G., Cousin, J.-M., Legrand, C., Abonnel, C.,
813 Lecoeur, F., Cayez, G., and Marizy, C.: An improved infrared carbon monoxide analyser for
814 routine measurements aboard commercial Airbus aircraft: technical validation and first scientific
815 results of the MOZAIC III programme, *Atmos. Chem. Phys.*, 3, 1551–1564, doi:10.5194/acp-3-
816 1551-2003, 2003.

817 Nie, W., Ding, A., Wang, T., Kerminen, V.-M., George, C., Xue, L., Wang, W., Zhang, Q., Petaja,
818 T., Qi, X., Gao, X., Wang, X., Yang, X., Fu, C., and Kulmala, M.: Polluted dust promotes new
819 particle formation and growth, *Sci. Rep.*, 4, 6634, doi:10.1038/srep06634, 2014.

820 Nilsson, E. D., Rannik, U., Kulmala, M., Buzorius, G., and O'Dowd, C. D.: Effects of continental
821 boundary layer evolution, convection, turbulence and entrainment, on aerosol formation,
822 *TellusB*, 53, 441–461, 2001.

823 O'Dowd, C., Monahan, C., and Dall'Osto, M.: On the occurrence of open ocean particle production
824 and growth events, *Geophys. Res. Lett.*, 37, L19805, doi:10.1029/2010GL044679, 2010.

825 Pace, G., di Sarra, A., Meloni, D., Piacentino, S., and Chamard, P.: Aerosol optical properties at
826 Lampedusa (Central Mediterranean). 1. Influence of transport and identification of different
827 aerosol types, *Atmos. Chem. Phys.*, 6, 697–713, doi:10.5194/acp-6-697-2006.

828 Pace, G., Junkermann, W., Vitali, L., di Sarra, A., Meloni, D., Cacciani, M., Cremona, G.,
829 Iannarelli, A. M., and Zanini, G.: On the complexity of the boundary layer structure and aerosol
830 vertical distribution in the coastal Mediterranean regions: a sea breeze, desert dust transport, and
831 free-tropospheric air intrusion case study in Southern, submitted to *TellusB*, 2015.

832 Parrish, D. D., Holloway, J. S., Trainer, M., Murphy, P. C., Fehsenfeld, F. C., and Forbes, G. L.:
833 Export of North America ozone pollution to the North Atlantic Ocean, *Science*, 259, 1436–1439,
834 1993.

835 Parrish, D. D., Trainer, M., Holloway, J. S., Yee, J. E., Warshawsky, M. S., Fehsenfeld, F. C.,
836 Forbes, G. L., and Moody, J. L.: Relationships between ozone and carbon monoxide at surface
837 sites in the North Atlantic region, *J. Geophys. Res.*, 103, 13,357– 13,376, 1998.

838 Pérez, C., Sicard, M., Jorba, O., Comeron, A., and Baldasano, J. M.: Summertime re-recirculations
839 of air pollutants over the North-Eastern Iberian coast observed from systematic EARLINET lidar
840 measurements in Barcelona, *Atmos. Environ.*, 38, 3983–4000, 2004.

841 Pérez, N., Pey, J., Castillo, S., Viana, M., Alastuey, A., and Querol, X.: Interpretation of the
842 variability of levels of regional background aerosols in the Western Mediterranean, *Sci. Tot.*
843 *Environ.*, 407, 527–540, 2008.

844 Petzold, A., Fiebig, M., Flentje, H., Keil, A., Leiterer, U., Schroder, F., Stifter, A., Wendisch, M.,
845 and Wendling, P.: Vertical variability of aerosol properties observed at a continental site during
846 the Lindenberg Aerosol Characterization Experiment (LACE 98), *J. Geophys. Res.*, 107, 8128,
847 doi:10.1029/2001JD001043, 2002.

848 Pey, J., Querol, X., and Alastuey, A.: Discriminating the regional and urban contributions in the
849 North-Western Mediterranean: PM levels and composition, *Atmos Environ*, 44, 1587–96, 2010.

850 Raut, J.-C., and Chazette, P.: Vertical profiles of urban aerosol complex refractive index in the
851 frame of ESQUIF airborne measurements, *Atmos. Chem. Phys.*, 8, 901–919, 2008.

852 Rose, C., Sellegri, K., Asmi, E., Hervo, M., Freney, E., Junninen, H., Duplissy, J., Sipilä, M.,
853 Kontkanen, J., Lehtipalo, K., and Kulmala, M.: Major contribution of neutral clusters to new
854 particle formation in the free troposphere, *Atmos. Chem. Phys. Discuss.*, 14, 18355–18388,
855 2014.

856 Salameh, T., Drobinski, P., Menut, L., Bessagnet, B., Flamant, C., Hodzic, A., and Vautard, R.:
857 Aerosol distribution over the western Mediterranean basin during a Tramontane/Mistral event,
858 *Ann. Geophys.*, 25, 2271–2291, 2007.

859 Sellegri, K., Laj, P., Venzac, H., Boulon, J., Picard, D., Villani, P., Bonasoni, P., Marinoni, A.,
860 Cristofanelli, P., and Vuillermoz, E.: Seasonal variations of aerosol size distributions based on
861 long-term measurements at the high altitude Himalayan site of Nepal Climate Observatory-
862 Pyramid (5079 m), Nepal, *Atmos. Chem. Phys.*, 10, 10679–10690, doi:10.5194/acp-10-10679-
863 2010, 2010.

864 Soriano, C., Baldasano, J. M., Buttler, W. T., and Moore, K.: Circulatory patterns of air pollutants
865 within the Barcelona air basin in a summertime situation: lidar and numerical approaches.
866 *Bound.-Lay. Meteorol.*, 98 (1), 33–55, 2001.

867 Spracklen, D. V., Carslaw, K. S., Kulmala, M., Kerminen, V.-M., Sihto, S.-L., Riipinen, I.,
868 Merikanto, J., Mann, G. W., Chipperfield, M. P., and Wiedensohler, A.: Contribution of particle
869 formation to global cloud condensation nuclei concentrations, *Geophys. Res. Lett.*, 35, L06808,
870 doi:10.1029/2007GL033038, 2008.

871 Stohl, A., Wotawa, G., Seibert, P., and Krompkolb, H.: Interpolation errors in wind fields as a
872 function of spatial and temporal resolution and their impact on different types of kinematic
873 trajectories, *J. Appl. Meteorol.*, 34, 2149–2165, 1995.

874 Velchev, K., Cavalli, F., Hjorth, J., Marmer, E., Vignati, E., Dentener, F., and Raes, F.: Ozone over
875 the Western Mediterranean Sea – results from two years of shipborne measurements, *Atmos.*
876 *Chem. Phys.*, 11, 675–688, doi:10.5194/acp-11-675-2011, 2011.

877 Wallace J.M., and Hobbs, P.V.: *Atmospheric science: an introductory survey* (2nd edition).
878 International Geophysics Series 92, Academic press, Burlington, 484pp, 2006.

879 Wehner, B., H. Siebert, A. Ansmann, F. Ditas, P. Seifert, F. Stratmann, A. Wiedensohler, A. 956
880 Apituley, R. A. Shaw, H. E. Manninen, and M. Kulmala (2010), Observations of turbulence
881 induced new particle formation in the residual layer, *Atmos. Chem. Phys.*, 10, 4319–4330, 958
882 doi:10.5194/acp-10-4319-2010.

883 Wiegner, M., Emeis, S., Freudenthaler, V., Heese, B., Junkermann, W., Munkel, C., Schäfer, K.,
884 Seefeldner, M., and Vogt, S.: Mixing layer height over Munich, Germany: variability and
885 comparisons of different methodologies, *J. Geophys. Res.*, 111, D13201,
886 doi:10.1029/2005JD006593, 2006.

887 Zhang, L., Jacob, D. J., Bowman, K. W., Logan, J. A., Turquety, S., Hudman, R. C., Li, Q., Beer,
888 R., Worden, H. M., Worden, J. R., Rinsland, C. P., Kulawik, S. S., Lampel, M. C., Shephard, M.

889 W., Fisher, B. M., Eldering, A., and Avery M. A.: Ozone-CO correlations determined by the
890 TES satellite instrument in continental outflow regions, *Geophys. Res. Lett.*, 33, L18804,
891 doi:10.1029/2006GL026399, 2006.
892
893
894
895

896 Tables

897 **Table 1.** Summary of information on the TRAQA and SAFMED flights.

898

Measurement campaign	Flight number	Date	Take off-landing time (UTC)	Departure-arrival	Geographic area investigated	Description
TRAQA 2012	V16	20/06/2012	13:12 – 16:34	Toulouse-Toulouse	Gulf of Lion	Test flight
	V17*	22/06/2012	09:01 – 12:54	Toulouse-Toulouse	South-western France (over land) and the Atlantic Ocean	Test flight, biogenic emissions.
	V18*	26/06/2012	07:13 – 09:18	Toulouse-Bastia	Gulf of Genoa	Export of pollution from Northern Italy/Pô Valley, north-westerly winds
	V19	26/06/2012	10:42 – 13:46	Bastia-Toulouse	Gulf of Genoa	Export of pollution from Northern Italy/Pô Valley, north-westerly winds
	V20	27/06/2012	04:07 – 08:00	Toulouse-Nimes	Sea area south of Marseille/Toulon	Export of pollution during a Mistral-Tramontane event
	V21	27/06/2012	09:39 – 13:16	Nimes-Toulouse	Western coast of Corsica	Export of pollution from Northern Italy/Pô Valley, north-westerly winds
	V22	29/06/2012	05:13 – 08:50	Toulouse-Bastia	Eastern coast of Corsica	Dust outbreak
	V23	29/06/2012	10:13 – 14:12	Bastia-Toulouse	Eastern and western coasts of Corsica	Dust outbreak
	V24	03/07/2012	13:19 – 17:12	Toulouse-Toulouse	Sea area north-east of Barcelona	Export of pollution from Barcelona, westerly/south-westerly winds
	V25	04/07/2012	07:18 – 10:54	Toulouse-Toulouse	Sea area south of Marseille/Toulon	Follow of Barcelona pollution plumes
	V26	04/07/2012	15:25 – 18:36	Toulouse-Toulouse	Gulf of Lion	Follow of Barcelona pollution plumes
	V27	06/07/2012	08:00 – 11:55	Toulouse-Toulouse	Sea area south of Marseille	Export of pollution during a moderate Mistral-Tramontane event
	V28	06/07/2012	14:01 – 17:45	Toulouse-Toulouse	Sea area south of Nice/Toulon	Export of pollution during a moderate Mistral-Tramontane event
	V29*	07/07/2012	08:19 – 10:59	Toulouse-Nimes	Southern France (over land)	Biogenic emissions
	V30	07/07/2012	13:03 – 17:10	Nimes-Toulouse	Gulf of Genoa	Export of pollution during a moderate Mistral-Tramontane event
	V31	10/07/2012	13:41 – 17:21	Toulouse-Toulouse	Eastern coast of Spain	Characterization of pollution near coastal

Mis en forme : Exposant

						sources
	V32	11/07/2012	11:23 – 14:48	Toulouse-Toulouse	Southeastern coast of France and Gulf of Genoa	Characterization of pollution near coastal sources
SAFMED 2013	V46	24/07/2013	10:34 – 13:06	Genoa-Cagliari	Gulf of Genoa and eastern coast of Corsica and Sardinia	Characterization of pollution plumes in the Gulf of Genoa, Corsica, and Sardinia; westerly/south-westerly winds
	V47*	24/07/2013	14:21 – 16:29	Cagliari-Genoa	Eastern coast of Corsica and Sardinia and Gulf of Genoa	Characterization of pollution plumes in the Gulf of Genoa, Corsica, and Sardinia; westerly/south-westerly winds
	V48	25/07/2013	13:12 – 16:02	Genoa-Ersa	Gulf of Genoa	Characterization of pollution in the Gulf of Genoa; westerly/south-westerly winds
	V49	27/07/2013	11:08 – 13:07	Genoa-Alghero	Central Italy (over land)	Characterization of pollution in central Italy
	V50*	27/07/2013	15:33 – 16:48	Alghero-Genoa	Eastern coast of Corsica and Gulf of Genoa	Characterization of pollution plumes in the Gulf of Genoa, Corsica, and Sardinia; westerly/south-westerly winds + dust outbreak
	V51	30/07/2013	13:05 – 15:50	Genoa-Ersa	Gulf of Genoa	Characterization of pollution in the Gulf of Genoa; very low north/north-westerly winds
	V52	01/08/2013	12:03 – 15:24	Genoa-Alghero	Western coast of Corsica	Characterization of pollution in western Corsica; export of pollution from Northern Italy/Pô Valley; north-easterly winds

* = No vertical profiles performed during these flights.

899
900
901
902
903
904
905
906

907 **Table 2.** Comparison of the number concentrations dN_{Aitken} (0.004-0.1 μm) and dN_{Acc} (0.1-1.0 μm)
 908 observed during the TRAQA/SAFMED field campaigns with those reported in literature for
 909 continental Europe. All literature data refer to airborne measurements.
 910

Atmospheric layer	Parameter	TRAQA/SAFMED	Literature over continental Europe
Free troposphere (FT)	dN_{Aitken} (scm^{-3})	0-19250	812-9149 ^b ; 0-980 ^c
	dN_{Acc} (scm^{-3})	34-3233	20-80 ^a ; 25-85 ^c ; 0-500 ^f
Boundary layer (BL)	dN_{Aitken} (scm^{-3})	4-22471	1037-31370 ^b ; 1000-20000 ^c ; 0-30000 ^d ; 0-19000 ^e
	dN_{Acc} (scm^{-3})	90-3215	70-560 ^a ; 10-50 ^c ; 400-1200 ^e ; 0-2000 ^f

911

912 ^a Petzold et al. (2002), Central Europe, July-August 1998; size range dN_{Acc} (>0.15 μm)

913 ^b Mallet et al. (2005), Southeastern France, June 2001; size range dN_{Aitken} (0.006-0.6 μm)

914 ^c Wiegner et al. (2006), Germany, May 2003; ; size range dN_{Aitken} (>0.01 μm), dN_{Acc} (>0.3 μm)

915 ^d Junkermann (2009), Po Valley, July-August 2002 and September-October 2003; ; size range dN_{Aitken} (>0.01 μm)

916 ^e Hamburger et al. (2012), central Europe, May 2008; size range dN_{Aitken} (0.004-0.15 μm), dN_{Acc} (>0.15 μm)

917 ^f Highwood et al. (2012), central Europe, May 2008; size range dN_{Aitken} (0.004-0.15 μm), dN_{Acc} (>0.15 μm)

918

919

920

921

922

923

924

925

926

927

928

929

930

931

932

933

934

935

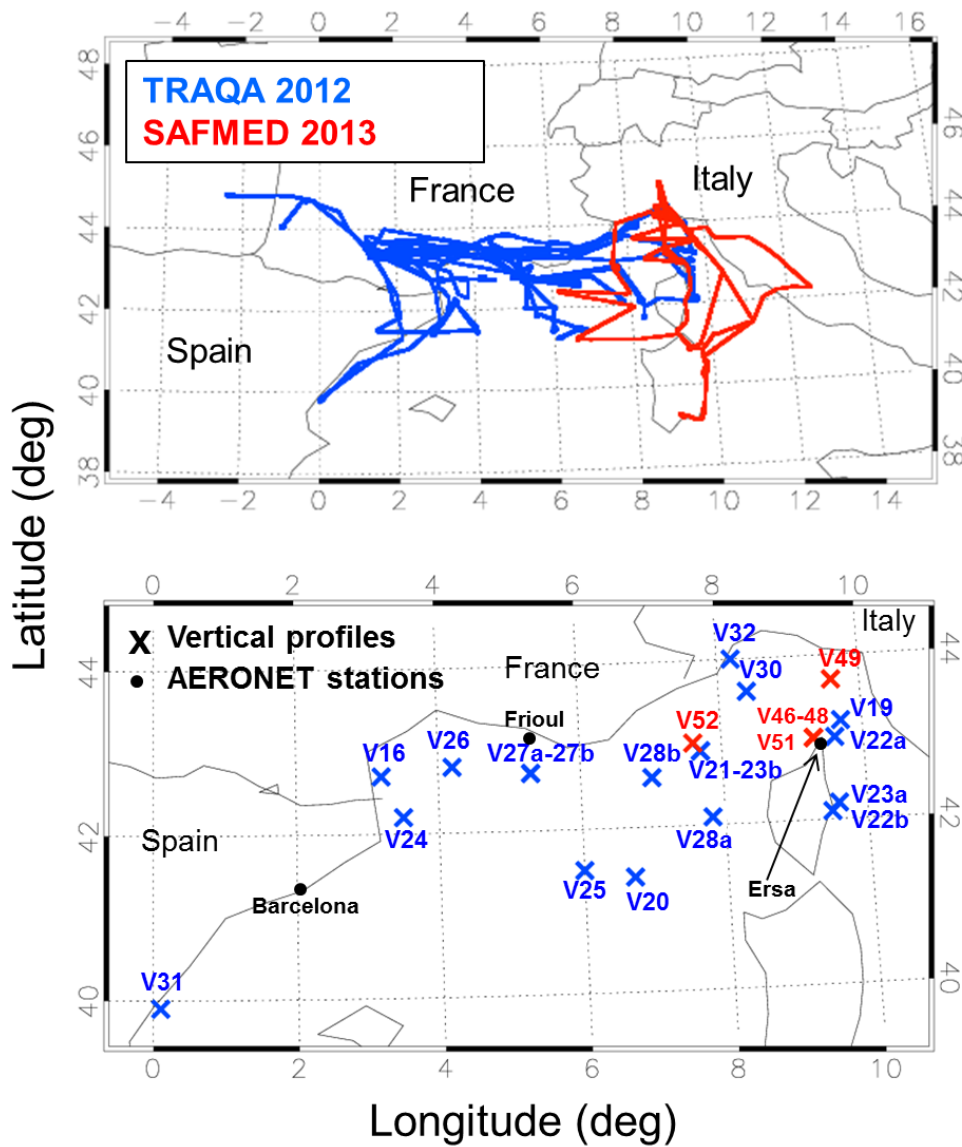
936

937

938

939 **Figures**

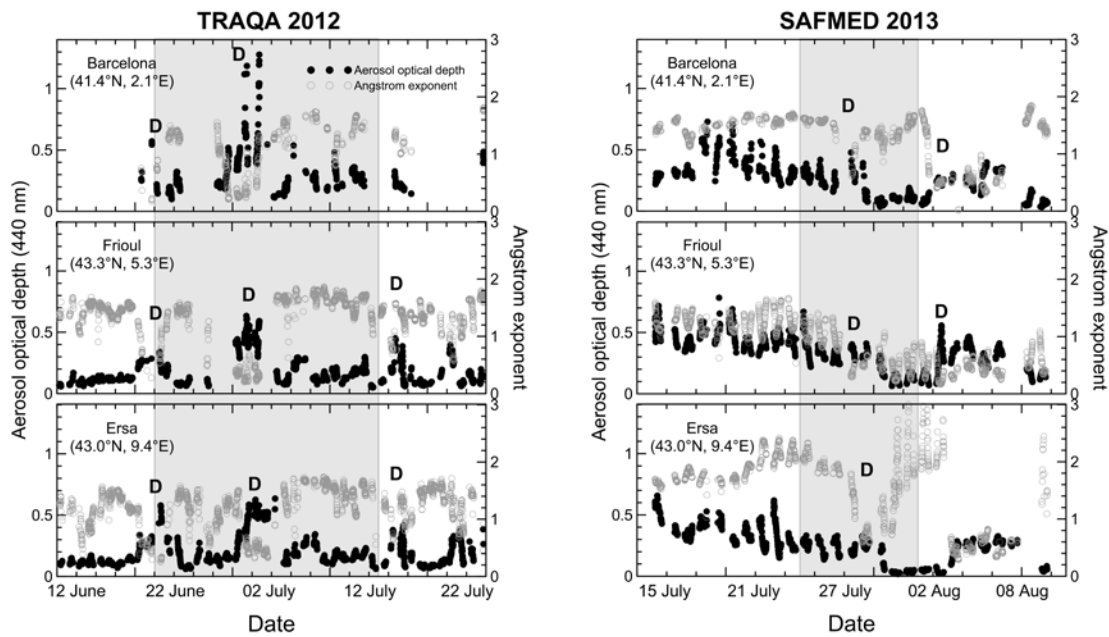
940 **Figure 1.** (Upper panel) Flight trajectories of the TRAQA (20 June - 13 July 2012) and the
941 SAFMED (24 July - 1 August 2013) campaigns. The aircraft was based in Toulouse (43°36'N,
942 1°26'E, France) during TRAQA and in Genoa (44°24'N, 8°55'E, Italy) during SAFMED. (Lower
943 panel) Zoom on the investigated area and geographical position of the different vertical soundings
944 analysed in this paper. The position of the three AERONET stations of Barcelona, Frioul, and Ers
945 considered in this study is also shown.
946
947



948
949
950
951

952 **Figure 2.** Aerosol optical depth at 440 nm (τ) and Ångström exponent (α) measured at the
 953 Barcelona, Frioul, and Ersa AERONET stations during the TRAQA 2012 (left panels) and the
 954 SAFMED 2013 (right panels) campaigns. The time period for the different plots is ± 10 days around
 955 the beginning/end of the two campaigns (data for the Barcelona station are not available over the
 956 entire period for 2012). The label D indicates the days affected by Saharan dust.
 957

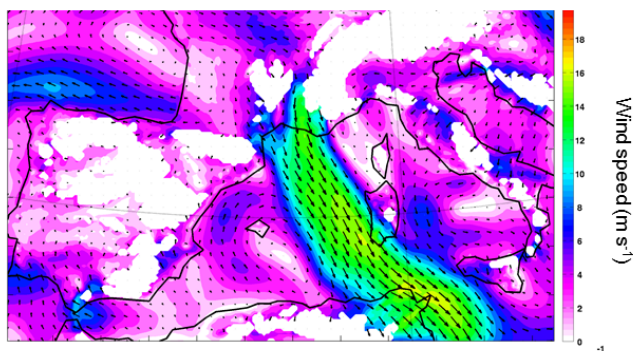
958
 959



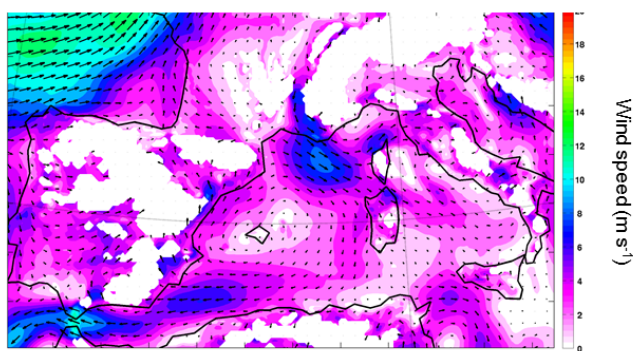
960
 961
 962
 963
 964
 965
 966
 967
 968
 969
 970
 971
 972
 973
 974
 975

976 **Figure 3.** Example of wind maps at 925 mbar for 26 June and 3 July 2012. The maps are obtained
977 from the WRF-Chem model (Weather Research and Forecasting – Chemistry) at 10-km horizontal
978 resolution.
979

a) 26 June 2012 12UT, 925 hPa



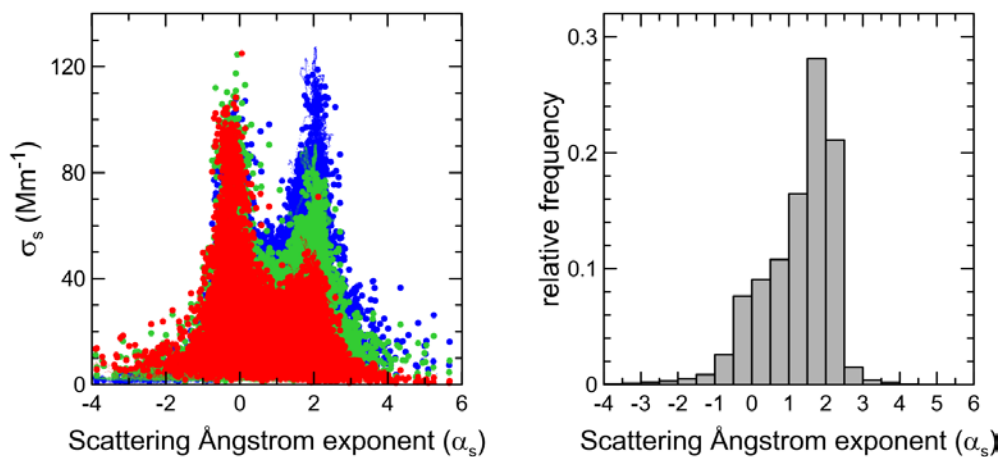
b) 03 July 2012 12UT, 925 hPa



980
981
982
983
984
985
986
987
988
989
990
991

992 **Figure 4.** (Left) Scattering coefficient σ_s at 450, 550, and 700 nm versus the scattering Ångstrom
993 exponent α_s . Cases with extremely negative (<-2) and positive (>4) values of α_s are always related
994 with very low scattering coefficients, and are likely due to instrumental noise under low scattering
995 conditions. (Right) Frequency of occurrence of α_s obtained considering vertical profiles data from
996 all TRAQA and SAFMED flights.

997



998

999

1000

1001

1002

1003

1004

1005

1006

1007

1008

1009

1010

1011

1012

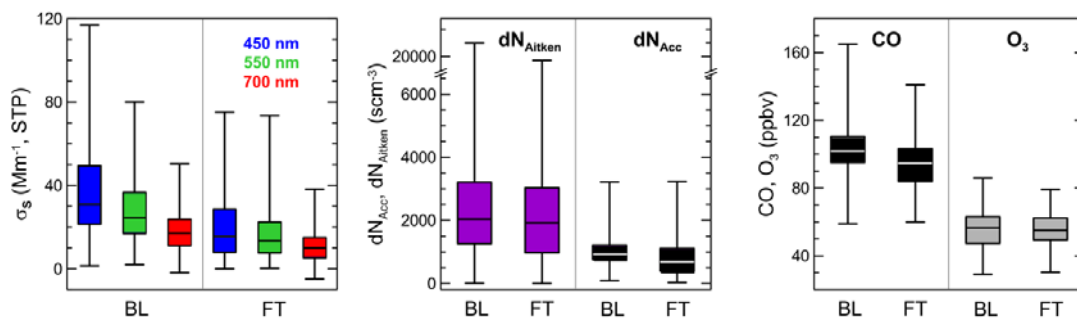
1013

1014

1015

1016

1017 **Figure 5.** Box and whisker plot of the aerosol scattering coefficient (σ_s) at 450, 550, and 700 nm,
 1018 particle concentration in the Aitken (dN_{Aitken}) and accumulation (dN_{Acc}) modes, and CO and O₃
 1019 measured within pollution plumes in the boundary layer (BL) and in the free troposphere (FT).
 1020
 1021



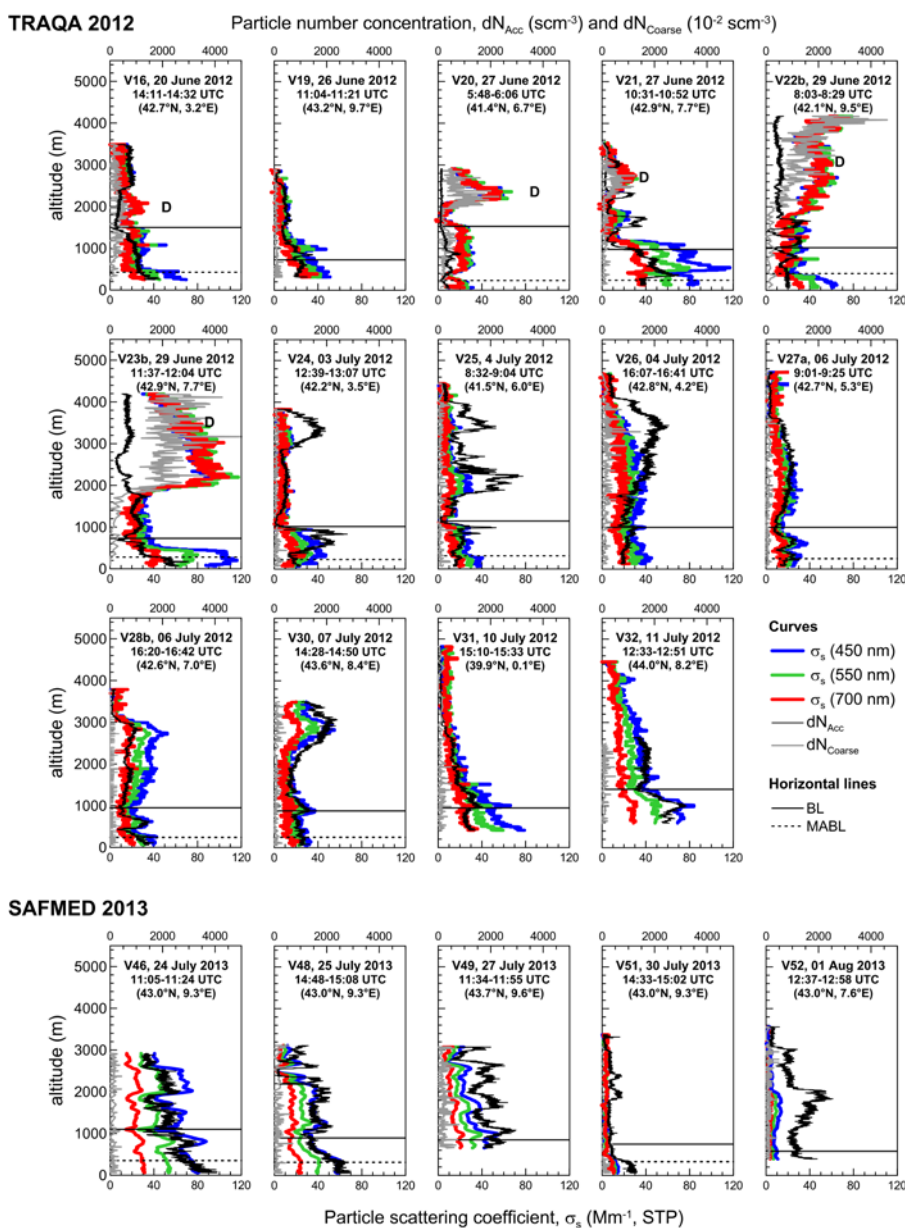
1022
 1023
 1024
 1025
 1026
 1027
 1028
 1029
 1030
 1031
 1032
 1033
 1034
 1035
 1036
 1037
 1038
 1039
 1040
 1041
 1042
 1043
 1044
 1045
 1046
 1047
 1048
 1049
 1050
 1051
 1052
 1053
 1054
 1055
 1056

1057 **Figure 6.** Vertical profiles of the spectral scattering coefficient σ_s at 450, 550, and 700 nm and
 1058 particle number concentration in the 0.1-1.0 μm (dN_{Acc}) and 1.0-4.0 μm (dN_{Coarse}) diameter ranges
 1059 observed during TRAQA and SAFMED. Data are reported at STP (standard temperature and
 1060 pressure, $T=293.15\text{ K}$ and $P=1013.25\text{ hPa}$). The heights of the top of the marine aerosol boundary
 1061 layer (MABL) and planetary boundary layer (BL) estimated from the meteorological profiles are
 1062 also indicated in the plots. The label D is used to identify the aerosol layers affected by Saharan
 1063 dust. For certain flights (V22, V23, V27, and V28) two vertical soundings were performed; the
 1064 letters “a” and “b” after the flight number in this plot specify if the considered data are taken from
 1065 the first or the second sounding, respectively.

Mis en forme : Exosant

Mis en forme : Indice

(* data for dN_{Coarse} are multiplied by 100 in the plot).

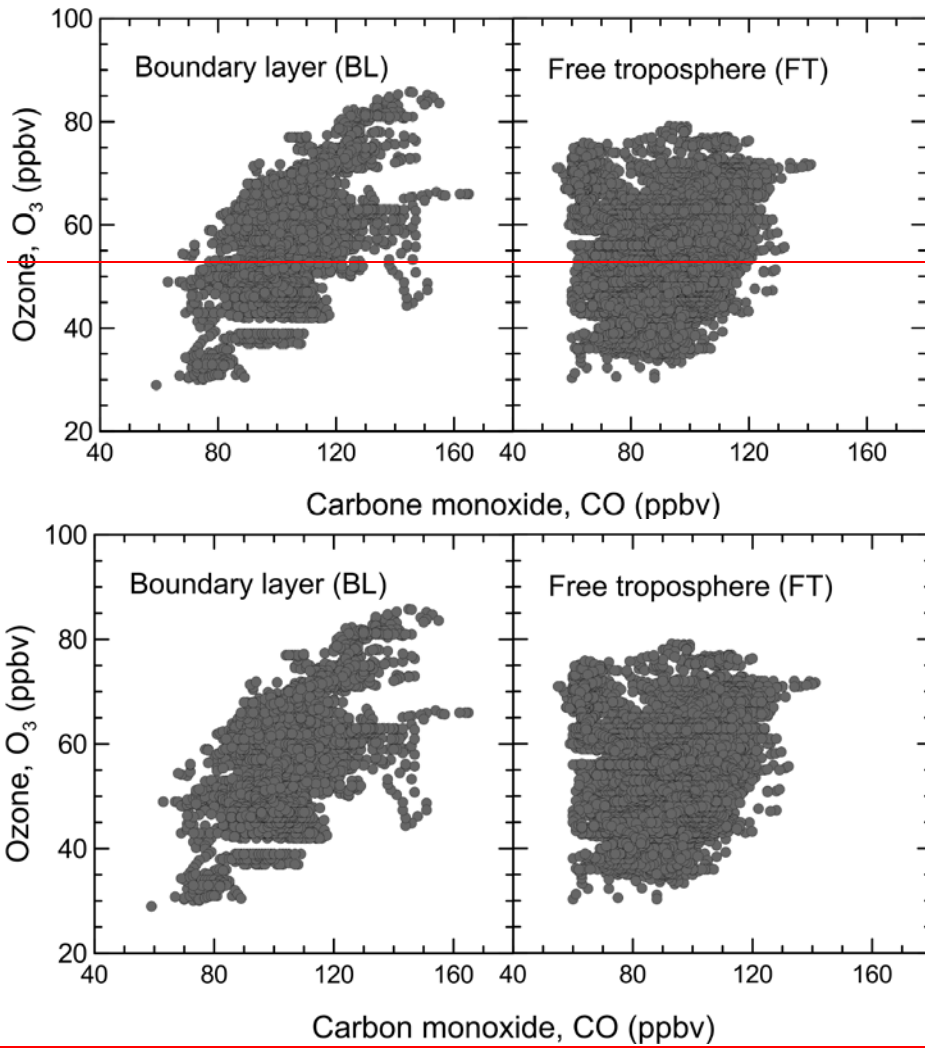


1068

47

1069
1070
1071
1072
1073

Figure 7. O₃ versus CO in the boundary layer (BL) and the free troposphere (FT) for all TRAQA and SAFMED vertical profiles (dust observations excluded).

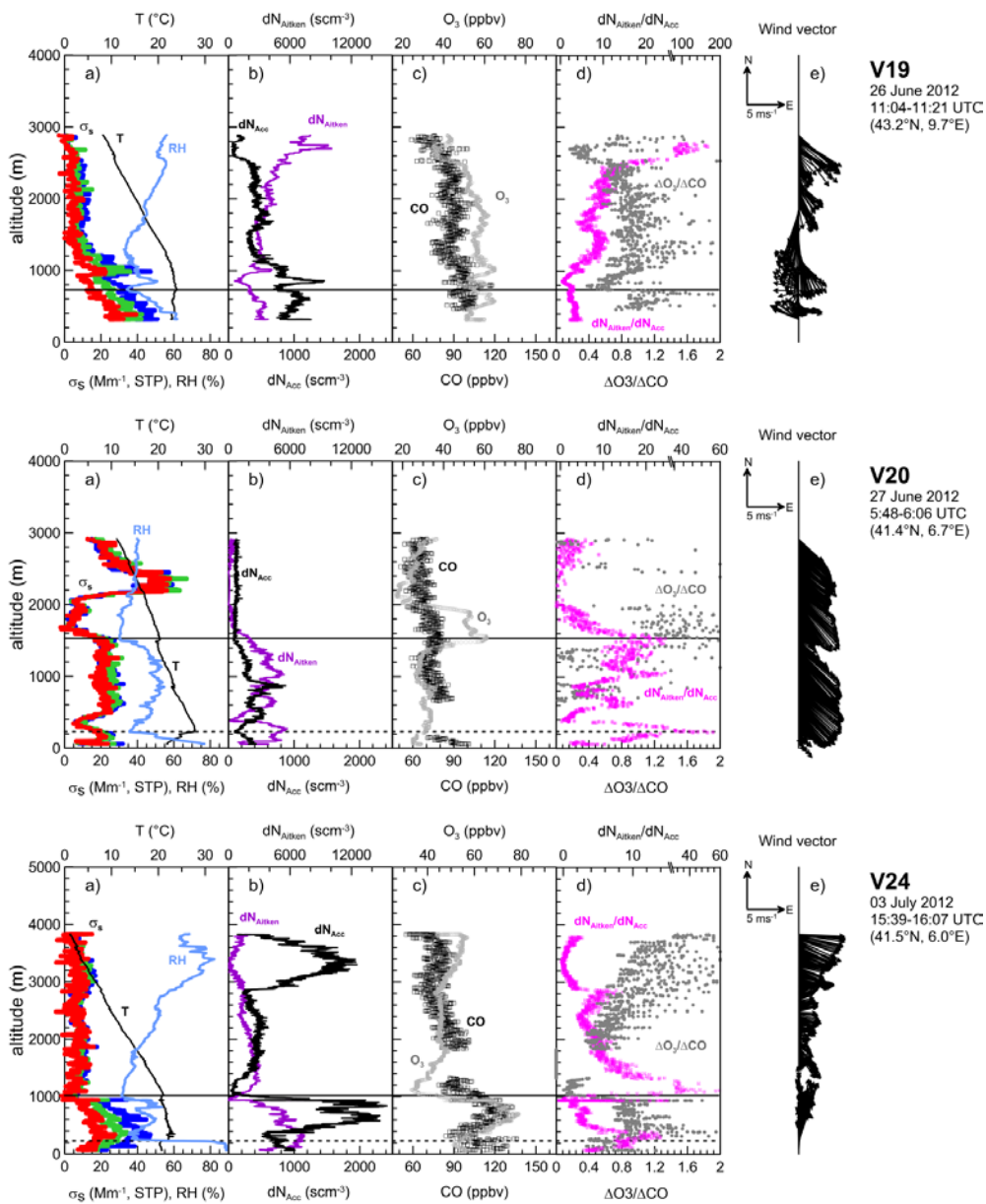


1074

1075
1076
1077
1078
1079
1080
1081
1082
1083
1084
1085
1086

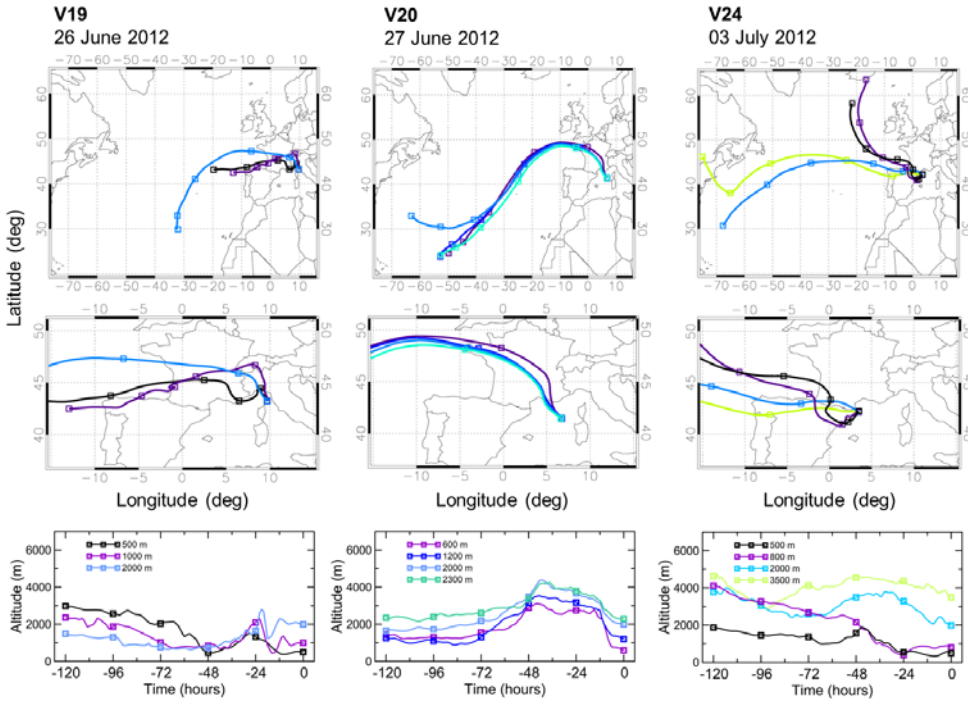
1087
1088
1089
1090
1091
1092
1093
1094
1095
1096
1097
1098
1099
1100
1101
1102
1103
1104
1105
1106
1107
1108
1109
1110
1111
1112
1113

Figure 8. Aerosol and trace gases vertical profiles for flights V19 (export from northern Italy/Po Valley), V20 (Mistral event), and V24 (export from the Barcelona area). The plots show the: (a) spectral scattering coefficient σ_s at 450, 550, and 700 nm (blue, green, and red lines, respectively), temperature (T, black line), and relative humidity (RH, light blue line); (b) particle number concentration in the 0.004-0.1 μm (dN_{Aitken} , purple line) and 0.1-1.0 μm (dN_{Acc} , black line) diameter ranges, (c) CO (black dots) and O₃ (grey dots) mixing ratios, (d) ozone enhancement factor $\Delta\text{O}_3/\Delta\text{CO}$ (grey dots) and Aitken to accumulation ratio $dN_{\text{Aitken}}/dN_{\text{Acc}}$ (pink dots) and (e) horizontal wind vector. The heights of the top of the MABL (dotted line) and BL (solid line) are also indicated.



1114

1115 **Figure 9.** Five-days backward air mass trajectories for the V19, V20, and V24 flights calculated
 1116 with the FLEXTRA model. The upper panel shows the trajectories over an extended latitude-
 1117 longitude region, while the central panel zooms on the Western Mediterranean area. The altitude of
 1118 the air masses and its temporal evolution along the five days trajectories is reported in the lower
 1119 panel of each plot.
 1120



1121
 1122
 1123
 1124
 1125
 1126
 1127
 1128
 1129
 1130
 1131
 1132
 1133
 1134
 1135

Figure 10. Vertical profiles of the accumulation and Aitken particle concentrations (dN_{Acc} , black line, and dN_{Aitken} , purple line), CO (black dots), O_3 (grey dots), and gradient Richardson number (Ri , green line) for flights a) V31, b) V28, c) V19, d) V26 and e) V23b. The horizontal lines indicate the height of the marine boundary layer MABL (dotted line) and the planetary boundary layer BL (continuous line), while the vertical lines indicate $Ri_{crit}=0.25$ and $Ri=1$ (continuous and dashed lines, respectively).

